Autophagy 10:11, 2036–2052; November 2014; © 2014 Taylor & Francis Group, LLC

Autophagy regulator BECN1 suppresses mammary tumorigenesis driven by WNT1 activation and following parity

Michelle Cicchini,[1,3] Rumela Chakrabarti,[4] Sameera Kongara,[1,3] Sandy Price,[1,3] Ritu Nahar,[3] Fred Lozy,[1,3] Hua Zhong,[3,5] Alexei Vazquez,[1,3] Yibin Kang,[1,4] and Vassiliki Karantza[1,2,3,†,*]

[1]Rutgers Cancer Institute of New Jersey; New Brunswick, NJ USA; [2]Department of Medicine; Division of Medical Oncology; Rutgers Robert Wood Johnson Medical School; New Brunswick, NJ USA; [3]Rutgers University; Piscataway, NJ USA; [4]Department of Molecular Biology; Princeton University; Princeton, NJ USA; [5]Department of Pathology; Rutgers Robert Wood Johnson Medical School; New Brunswick, NJ USA

[†]Current affiliation: Merck Research Laboratories; Rahway, NJ USA

Keywords: Beclin 1, Keratin 6, WNT1, TNFSF11, TNFRSF11A, TNR11, TNF11, basal-like breast cancer, TNBC, parity, NFKB

Abbreviations: 8-O-dG, 8-oxo-7, 8-dihydroguanine; ATG, autophagy-related; BECN1, Beclin 1, autophagy-related; BSA, bovine serum albumin; CASP3, caspase 3; CD24, cluster of differentiation 24; DAPI, 4′, 6-diamidino-2-phenylindole; DFS, disease-free survival; DMEM, Dulbecco's modified Eagle's medium; E, 17b-estradiol; EGF, epidermal growth factor; EGFP, enhanced green fluorescent protein; EGFR/ERBB1, epidermal growth factor receptor; EM, electron microscopy; EMT, epithelial-to-mesenchymal transition; ESR1, estrogen receptor 1; ERBB2, v-erb-b2 avian erythroblastic leukemia viral oncogene homolog 2; FACS, fluorescence activated cell sorting; FGF2/bFGF, fibroblast growth factor 2 (basic); GSEA, gene set enrichment analysis; H&E, hematoxylin & eosin; HR, hormone receptor; IF, immunofluorescence; IHC, immunohistochemistry; IL, interleukin; iMMECs, immortalized mouse mammary epithelial cells; ITGB1/CD29, Integrin, beta 1 (fibronectin receptor, beta polypeptide, antigen CD29 includes MDF2, MSK12); ITGB3/CD61, integrin, beta 3 (platelet glycoprotein IIIa, antigen CD61); KRT, keratin; LIN$^-$, lineage negative (CD31$^-$ CD45$^-$ LY76$^-$); MAP1LC3B/LC3B, microtubule-associated protein 1 light chain 3 beta; MaPC, mammary progenitor cell; MaSC, mammary stem cell; MEC, mammary epithelial cell; MEGM, mammary epithelial growth medium; MGs, mammary glands; MKI67, marker of proliferation Ki-67; MMTV, mouse mammary tumor virus; NFKB/NFkB, nuclear factor of kappa light polypeptide gene enhancer in B-cells; p-KRT8/p-K8, phosphorylated Keratin 8; PBS, phosphate-buffered saline; PECAM1/CD31, platelet/endothelial cell adhesion molecule 1; PI, propidium iodide; PGR, progesterone receptor; PTPRC/CD45, protein tyrosine phosphatase, receptor type, C; RELA/P65, v-rel avian reticuloendotheliosis viral oncogene homolog a; ROS, reactive oxygen species; SD, standard deviation; SNPs, single nucleotide polymorphisms; SQSTM1/p62, sequestosome1; TEBs, terminal end buds; LY76/TER119, lymphocyte antigen 76; TNBCs, triple-negative breast cancers; TNF, tumor necrosis factor; TNFRSF11A/TNR11/RANK, tumor necrosis factor receptor superfamily, member 11a, NFKB activator; TNFSF11/TNF11/RANKL, tumor necrosis factor (ligand) superfamily, member 11; TP53 (TRP53 in mice), tumor protein p53 (transformation related protein 53 in mice); WNT1, wingless-Type MMTV integration site family, member 1.

Earlier studies reported allelic deletion of the essential autophagy regulator *BECN1* in breast cancers implicating *BECN1* loss, and likely defective autophagy, in tumorigenesis. Recent studies have questioned the tumor suppressive role of autophagy, as autophagy-related gene (*Atg*) defects generally suppress tumorigenesis in well-characterized mouse tumor models. We now report that, while it delays or does not alter mammary tumorigenesis driven by *Palb2* loss or ERBB2 and PyMT overexpression, monoallelic *Becn1* loss promotes mammary tumor development in 2 specific contexts, namely following parity and in association with wingless-type MMTV integration site family, member 1 (WNT1) activation. Our studies demonstrate that *Becn1* heterozygosity, which results in immature mammary epithelial cell expansion and aberrant TNFRSF11A/TNR11/RANK (tumor necrosis factor receptor superfamily, member 11a, NFKB activator) signaling, promotes mammary tumorigenesis in multiparous FVB/N mice and in cooperation with the progenitor cell-transforming WNT1 oncogene. Similar to our *Becn1*$^{+/-}$;MMTV-*Wnt1* mouse model, low *BECN1* expression and an activated WNT pathway gene signature correlate with the triple-negative subtype, TNFRSF11A axis activation and poor prognosis in human breast cancers. Our results suggest that BECN1 may have nonautophagy-related roles in mammary development, provide insight in the seemingly paradoxical roles of BECN1 in tumorigenesis, and constitute the basis for further studies on the pathophysiology and treatment of clinically aggressive triple negative breast cancers (TNBCs).

*Correspondence to: Vassiliki Karantza; Email: vassiliki.karantza@merck.com
Submitted: 03/28/2014; Revised: 07/31/2014; Accepted: 08/08/2014
http://dx.doi.org/10.4161/auto.34398

Introduction

Macroautophagy (hereforth referred to as autophagy) is a catabolic process whereby protein aggregates and damaged organelles are constitutively degraded in lysosomes.[1] Cells also activate autophagy to survive under stress by recycling cytoplasmic material for energy production and biomolecular synthesis.[1] Defective autophagy was first implicated in tumorigenesis with the report that the essential autophagy regulator *BECN1*/Beclin1 is allelically deleted in human cancers, including breast cancer,[2] restoration of BECN1 expression in MCF7 breast carcinoma cells compromises xenograft tumor growth,[3] and *Becn1*$^{+/-}$ mice develop spontaneous lung and liver carcinomas, lymphomas, and mammary hyperplasias.[4,5] Furthermore, apoptosis-defective *Becn1*$^{+/-}$ immortalized mouse mammary epithelial cells (iMMECs) are more tumorigenic in nude mice, accumulate DNA damage and are more genomically unstable than their wild-type counterparts.[6] Recently, work from Rosenfeldt and colleagues eloquently describes synergy between defective autophagy and tumor protein 53 (*TP53*/*Trp53*/*p53,* note that the mouse nomenclature is *Trp53,* but we use the *TP53* acronym hereafter to refer to both the human and mouse genes/proteins for simplicity*)* loss in KRAS (Kirsten rat sarcoma viral oncogene homolog)-driven pancreatic cancer,[7] while studies investigating the role of functional autophagy in ERBB2 (v-erb-b2 avian erythoblastic leukemia viral oncogene homolog 2)-positive and EGFR/ERBB1 (epidermal growth factor receptor)-expressing cells also implicate autophagy suppression in cell transformation driven by these oncogenes in mammary[8] and lung[9] epithelium, respectively.

Seemingly contradicting the results described above, several studies have reported that functional autophagy is required for tumorigenesis and tumor progression in some contexts.[7,10-14] Recent publications shed light on the role of BECN1, and autophagy in general, in mammary physiology, as ATG proteins have been found important for breast cancer stem cell maintenance[10] and dead cell clearance in mammary involution.[15] The role of BECN1 in mammary tumorigenesis is likely complex, as mammary glands (MGs) from *Becn1*$^{+/-}$ mice exhibit increased proliferation in puberty and hyperplasias with age, but no mammary tumors.[4] Furthermore, monoallelic *Becn1* loss does not have an impact on ERBB2- or PyMT-driven mammary tumorigenesis,[8] whereas it delays tumor formation due to mammary gland-specific biallelic *Palb2* deletion in a wild-type *Tp53* background.[13] The tumor-suppressive role of BECN1 in tumorigenesis has also recently been challenged by the finding that in human breast and ovarian cancers, large genomic deletions encompassing both *BRCA1* and *BECN1*, and deletions of only *BRCA1* but not *BECN1*, are observed.[16]

Our earlier study demonstrates that phosphorylated keratin 8 (p-KRT8) accumulates in autophagy-deficient iMMECs, tissues, and tumors, implicating autophagy in keratin homeostasis.[17] Building on this work, we now report that *Becn1*$^{+/-}$, compared with *Becn1*$^{+/+}$, iMMECs and iMMEC-generated tumors also exhibited KRT6 (keratin 6) upregulation. KRT6 is not only a basal cell marker in skin and mammary tissue, but also a marker for bipotent mammary progenitor cells and for cells with increased tumorigenic potential.[18,19] We also report that KRT6-positive cells, likely representing bipotent mammary progenitor cells, are aberrantly present in MGs from postpubertal *Becn1*$^{+/-}$ mice. Furthermore, we demonstrate that monoallelic *Becn1* loss results in augmented mammary stem and progenitor cell activities and TNFRSF11A-NFKB axis upregulation; it also promotes mammary tumor development following parity and accelerates WNT1-driven mammary tumorigenesis, which itself involves progenitor cell transformation.[18,20] Thus, our studies elucidate 2 physiologically relevant contexts in which monoallelic *Becn1* loss promotes mammary tumorigenesis, giving rise to tumors with basal-like characteristics.

Results

Monoallelic *Becn1* loss results in KRT6 upregulation in mammary epithelial cells and tissues

Apoptosis-defective *Becn1*$^{+/-}$ iMMECs have previously been reported to be more tumorigenic in nude mice than their *Becn1*$^{+/+}$ counterparts.[6] To investigate *Becn1* genotype-specific differences in iMMECs and iMMEC-generated mammary tumors in nude mice, we performed gene expression analysis, which revealed that KRT6 was upregulated in *Becn1*$^{+/-}$ iMMECs (**Fig. 1A and B**) and, to an even higher and significant degree, in *Becn1*$^{+/-}$ iMMEC-generated allograft tumors (**Fig. 1A and C**). These tumors also displayed increased KRT14 expression compared with tumors resulting from orthotopic implantation of *Becn1*$^{+/+}$ iMMECs (**Fig. 1C**), further indicating an association between monoallelic *Becn1* loss and basal keratin expression in mammary tumor cells. This finding is in agreement with our recently published study, which reports that low BECN1 mRNA levels correlate with the basal-like and ERBB2, but not luminal, breast cancer subtypes.[8]

To exclude the possibility that KRT6 upregulation in *Becn1*$^{+/-}$ iMMECs and iMMEC-generated tumors resulted from the process of mammary epithelial cell (MEC) immortalization,[6] we investigated KRT6 expression in MGs from *Becn1*$^{+/+}$ and *Becn1*$^{+/-}$ mice. As previously reported,[21] KRT6 was detected in MGs from pubertal wild-type mice, whereas hardly any KRT6-positive cells were seen in MGs from aged wild-type mice (**Fig. 1D**). Mammary epithelium from pubertal *Becn1*$^{+/-}$ mice exhibited uniformly robust KRT6 expression, whereas KRT6-positive, not costaining with the luminal cytokeratin KRT8, cells were observed in MGs from aged *Becn1*$^{+/-}$ mice (**Fig. 1D**).

Since bipotent mammary progenitor cells express KRT6,[19] we examined whether KRT6-positive cells observed in MGs from older *Becn1*$^{+/-}$ mice also expressed mammary stem cell (MaSC) and progenitor cell markers.[22,23] We indeed found that these cells costained with the MaSC and progenitor cell marker CD24 (cluster differentiation 24) and expressed low levels of the MaSC marker CD29/integrin-β1 (cluster differentiation 29) (**Fig. 1E**), thus suggesting that monoallelic *Becn1* loss leads to accumulation of KRT6-positive bipotent mammary progenitor cells.

Monoallelic *Becn1* loss results in accelerated mammary fat pad filling and excessive ductal side-branching

In agreement with earlier results using a different *Becn1*$^{+/-}$ transgenic line,[4] we also detected increased proliferation in

mammary ducts and terminal end buds (TEBs) from 5-wk-old *Becn1*$^{+/-}$ mice[5] (**Fig. S1A and S1B**); apoptosis rates were similar (**Fig. S1C and S1D**). Consistent with the partially defective autophagic response observed in *Becn1*$^{+/-}$ iMMECs under metabolic stress,[6] lower levels of MAP1LC3B/LC3B (microtubule-associated protein 1 light chain 3 β) and accumulation of SQSTM1/p62 (sequestosome 1) were observed in MGs from *Becn1*$^{+/-}$ mice (**Fig. S1E and S1F**).

Systematic examination of MGs from cohoused *Becn1*$^{+/+}$ and *Becn1*$^{+/-}$ littermates revealed that 6.5-wk-old *Becn1*$^{+/-}$ mice exhibited accelerated mammary fat-pad filling and increased ductal side-branching (**Fig. 2A and B**). The latter phenotype persisted and was further accentuated in MGs from 6-mo-old nulliparous *Becn1*$^{+/-}$ mice (**Fig. 2C**, upper panel); at that age, *Becn1*$^{+/-}$ mice also exhibited mammary hyperplasias (**Fig. 2C**, lower panel). The difference in ductal side-branching in MGs from *Becn1*$^{+/+}$ and *Becn1*$^{+/-}$ mice became less pronounced by 12 mo of age (**Fig. 2D**), possibly indicating that increased ductal side-branching may be a hormonally regulated phenotype.

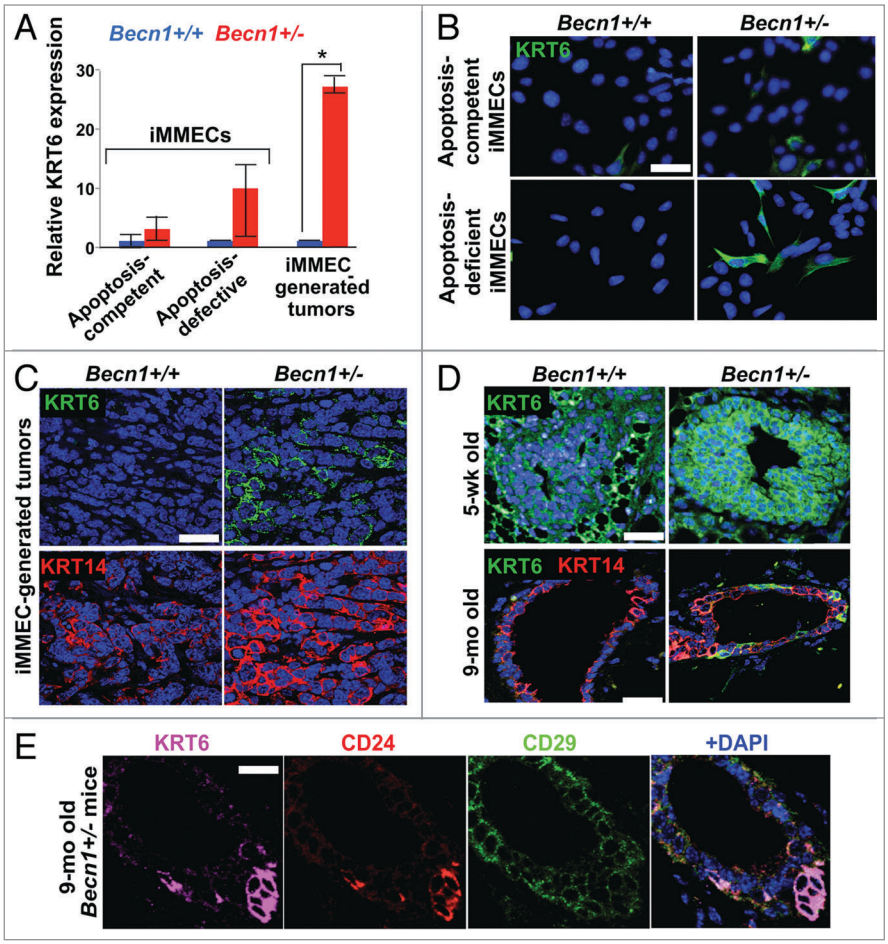

Figure 1. Monoallelic *Becn1* loss results in KRT6 upregulation in mammary epithelial cells and tissues. (**A**) Microarray analysis was performed on samples (three each) of *Becn1*$^{+/+}$ and *Becn1*$^{+/-}$ apoptosis-competent and apoptosis-defective iMMECS, as well as mammary tumors derived from orthotopic implantation of apoptosis-defective iMMECs in nude mice. *KRT6* expression relative to that in apoptosis-competent *Becn1*$^{+/+}$ iMMECs is presented as means ± SDs (n = 3). (**B–D**) *Becn1*$^{+/+}$ (left) and *Becn1*$^{+/-}$ (right) with DAPI (blue) by IF: (**B**) More KRT6-expressing cells are seen in *Becn1*$^{+/-}$ apoptosis-competent iMMECs (top) and *Becn1*$^{+/-}$ apoptosis-defective iMMECs (bottom) under normal growth conditions. (**C**) More KRT6-expressing (green, top) and KRT14-expressing (red, bottom) cells are seen in allograft mammary tumors generated by *Becn1*$^{+/-}$ apoptosis-defective iMMECs. (**D**) MGs from 5-wk-old (top) and 9-mo-old (bottom) *Becn1*$^{+/-}$ mice reveals increased number of KRT6-positive (green) cells that are not KRT8-positive (red). (**E**) Costaining for KRT6 (purple), CD24 (red), CD29 (green) in MGs from 9-mo-old *Becn1*$^{+/-}$ mice reveals that KRT6-positve cells colocalize with mammary progenitor cell markers. Scale bar: (**B and D**) 30 μm; (**C and E**) 37.5 μm.

Monoallelic *Becn1* loss results in functionally enriched mammary stem and progenitor cell populations

Faster mammary fat pad filling and excessive ductal side-branching result from increased mammary stem and progenitor cell populations/activity, respectively.[22] We utilized fluorescence-activated cell sorting (FACS) to isolate PI$^-$ LIN$^-$ CD24$^+$ CD29^{hi}, i.e. mammary stem cell (MaSC)-containing, and PI$^-$ LIN$^-$ CD24$^+$ CD29^{lo}, i.e. mammary progenitor cell (MaPC)-containing, populations[22] from cohoused *Becn1*$^{+/+}$ and *Becn1*$^{+/-}$ littermates. Although the relative proportions of MaSC-, MaPC-, and CD61 (cluster differentiation 61)$^+$ luminal progenitor cell-containing populations[22-24] were similar between the 2 genotypes (**Fig. S2A and S2B**), MGs from *Becn1*$^{+/-}$ mice consistently demonstrated higher MaSC and MaPC activities by in vitro and in vivo functional assays (**Fig. 3**; **Fig. S2C and S2D**). Specifically, CD24$^+$ CD29^{hi} *Becn1*$^{+/-}$ MECs exhibited increased MaSC activity, as measured by primary and limiting dilution mammosphere (**Fig. 3A**, left and right panel, respectively) and 3D colony-formation (**Fig. 3B**) assays.[23,25] Furthermore, CD24$^+$ CD29^{lo} *Becn1*$^{+/-}$ MECs exhibited increased MaPC activity (**Fig. 3C**), as measured by number of colonies formed in 2D-matrigel assays.[23,25]

The in vivo stem/progenitor cell activity of CD24$^+$ CD29^{hi} *Becn1*$^{+/+}$ and *Becn1*$^{+/-}$ MECs was evaluated by contralateral transplantation of these cells into cleared 4th mammary fat pads of wild-type mice.[22] CD24$^+$ CD29^{hi} *Becn1*$^{+/-}$ MECs consistently resulted in higher number of successful (i.e. giving rise to mammary outgrowths) transplantations (**Fig. 3D**; **Fig. S2C and S2D**). Six weeks post-transplantation, comparison of similarly filled fat pads revealed that CD24$^+$ CD29^{hi} *Becn1*$^{+/-}$ MECs gave rise to outgrowths with more extensive side-branching than

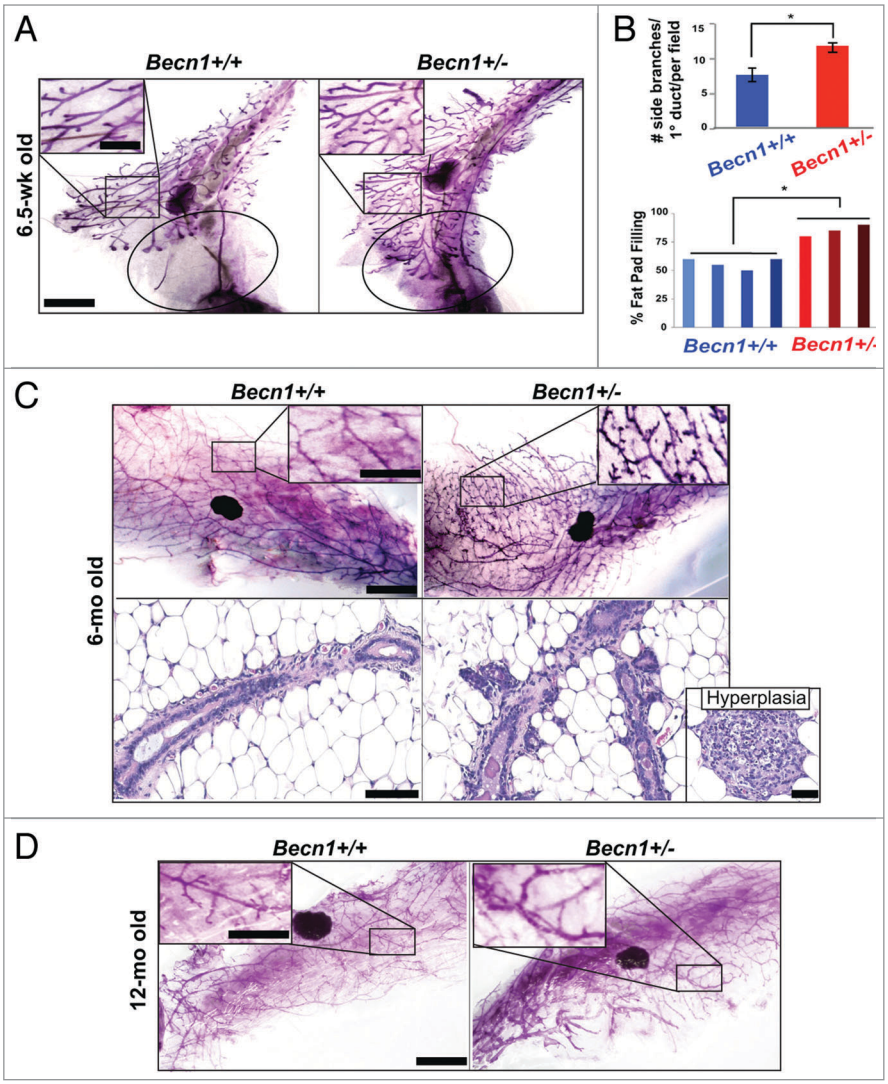

Figure 2. Monoallelic *Becn1* loss results in accelerated mammary fat pad filling and excessive ductal side-branching. (**A–D**) Analysis of mouse mammary epithelium from *Becn1*$^{+/+}$ (left) and *Becn1*$^{+/-}$ (right) mice (n = 3 to 5): (**A**) MG whole mounts from 6.5-wk-old mice, with circle identifying an unfilled (left) vs. filled (right) fat pad and (**B**) (top) quantification of number of side-branches per primary branch per field and (bottom) quantification of percentage of mammary fat pad 4 filled with epithelium. Three MG specimen per genotype from cohoused *Becn1*$^{+/+}$ and *Becn1*$^{+/-}$ littermates were evaluated. Results are presented as means ± SDs. (**C**) MG whole mounts (top) and hematoxylin and eosin staining of MG sections (bottom) from 6-mo-old mice, with mammary hyperplasia in separate insert. (**D**) MG whole mounts from 12-mo-old mice. Scale bar: (**A, C,and D**) 5 mm for whole mounts; (**A, C, and D**) 2 mm for whole mount enlargements. Scale bar: (**C**) 100 μm for H&Es; 200 μm for hyperplasia. *$P < 0.05$ by a 2-tailed Student *t* test.

CD24^{+} CD29^{hi} *Becn1*$^{+/+}$ MECs (**Fig. 3E**). This phenotype was similar to that observed in MGs from *Becn1*$^{+/-}$ mice (**Fig. 2**), suggesting that transplantation of MaSC-containing *Becn1*$^{+/-}$ MECs in wild-type mice sufficiently reproduced the side-branching phenotype observed in native MGs from *Becn1*$^{+/-}$ mice, where all cell types (MECs and stroma) are missing one *Becn1* allele.

Since transplantations of CD24^{+} CD29^{hi} *Becn1*$^{+/+}$ and *Becn1*$^{+/-}$ MECs were performed in wild-type recipient mice, we examined the autophagy status of resulting outgrowths and found that similar to MGs from *Becn1*$^{+/-}$ mice (**Fig. S1E and S1F**), CD24^{+} CD29^{hi} *Becn1*$^{+/-}$ MEC-generated outgrowths exhibited LC3B expression decrease and SQSTM1 accumulation (**Fig. S2E and S2F**). Furthermore, similar to MGs from *Becn1*$^{+/-}$ mice (**Fig. S1A and S1B**), proliferation rates in TEBs and mammary ducts were significantly higher in outgrowths derived from CD24^{+} CD29^{hi} *Becn1*$^{+/-}$ MEC transplantation (**Fig. 4A and B**). In contrast to similar apoptosis rates observed in native glands (**Fig. S1C and S1D**), in CD24^{+} CD29^{hi} *Becn1*$^{+/-}$ MEC-generated outgrowths, apoptosis was suppressed (**Fig. 4C and D**), possibly due to enrichment in more apoptosis-resistant MaSCs and MaPCs.

MEC subpopulations exhibit different levels of autophagic activity

Given that monoallelic *Becn1* loss resulted in deregulation of the mammary hierarchy, thus implicating BECN1, and possibly autophagy in general, in mammary differentiation, we isolated MEC populations from wild-type mice, as described above, and examined basal autophagy in these populations by electron microscopy (EM)[17] (**Fig. S3**). The CD24^{+} CD29^{hi} population exhibited paucity in mitochondria, autophagosomes, and other cytoplasmic organelles (**Fig. S3**, left panel), whereas the CD24^{+} CD29^{lo} population showed high autophagic activity, as illustrated by the presence of numerous autophagosomes (**Fig. S3**, middle panel). Interestingly, the autophagosomal cargo was different between CD24^{+} CD29^{hi} and CD24^{+} CD29^{lo} MECs; in the former (MaSC-containing) population, autophagosomes appeared largely carrying mitochondria, while in the latter (progenitor cell-containing) population, diverse cargo was observed in autophagosomes. Lastly, CD24^{-} MECs contained fewer autophagosomes than the CD24^{+} CD29^{lo} population, but more than the CD24^{+} CD29^{hi} compartment, and more mitochondria than both other MEC populations examined (**Fig. S3**, right panel). High autophagy induction in CD24^{+} CD29^{lo} MECs, though not a proof, suggests that autophagy may play a significant role in mammary differentiation, which is also accompanied by enrichment in mitochondria.

Krt14-driven biallelic *Atg7* deletion delays mammary fat pad filling, without altering ductal side-branching

In an effort to investigate whether the increased ductal side-branching and enriched MaSC and progenitor cell activities

observed in MGs from *Becn1*$^{+/-}$ mice were secondary to defective autophagy associated with monoallelic *Becn1* loss or to a nonautophagy-related BECN1 function, we generated mice with conditional biallelic deletion of the essential autophagy regulator *Atg7*[26] utilizing *Krt14* promoter-driven expression of CRE recombinase.[27] In agreement with prior studies showing that *Atg7* is not haploinsufficient for autophagy deficiency or other phenotypes,[26] we found that MGs from *Atg7*$^{+/+}$ and *Atg7*$^{F/+}$;*Krt14-Cre* mice displayed similar morphological characteristics (data not shown).

In MGs from *atg7*$^{F/F}$;*Krt14-Cre* mice, *Atg7* deletion and defective autophagy status were confirmed (**Fig. S4A and S4B**). In contrast to our observations in developing MGs from *Becn1*$^{+/-}$ mice (**Fig. 2A and B**), whole MG mounts revealed no difference in ductal side-branching between *Atg7*$^{+/+}$ and *atg7*$^{F/F}$;*Krt14-Cre* mice and, more impressively, showed delayed—rather than accelerated—fat pad filling in 6.5-wk-old *atg7*$^{F/F}$;*Krt14-Cre* mice (**Fig. S4C and S4D**). While proliferation rates were similar, increased apoptosis was detected in MGs from *atg7*$^{F/F}$;*Krt14-Cre* compared with *Atg7*$^{+/+}$ mice (**Fig. S4E and S4F**). Furthermore, KRT6, KRT8, and KRT14 levels were comparable in MGs from *atg7*$^{F/F}$;*Krt14-Cre* and *Atg7*$^{+/+}$ mice (**Fig. S4G and S4H**). Although functional in vitro and in vivo studies for MaSC and progenitor cell activities in *Atg7*$^{+/+}$ and *Atg7*-null CD24^{+} CD29^{hi} and CD24^{+} CD29^{lo} MECs were not performed, decreased mammary fat pad filling in pubertal MGs from *atg7*$^{F/F}$;*Krt14-Cre* mice suggests, at least partial, impairment of MaSC or progenitor cell function in association with MEC-specific biallelic *Atg7* deletion, and points to a nonautophagy-related role of BECN1 in mammary differentiation. Alternatively, and together with the evidence for high autophagic activity during mammary epithelial differentiation (**Fig. S3**) and the mammary phenotypes observed in MGs from *Becn1*$^{+/-}$ mice (Figs. 1, 2, and 3), it raises the possibility of a dose-dependent requirement for functional autophagy in MaSC and progenitor cell maintenance. If this is the case, partial autophagy deficiency may affect mammary cell hierarchy differently than a more severe autophagy defect. Further investigation of these 2 not necessarily mutually exclusive, mechanistic possibilities will be needed.

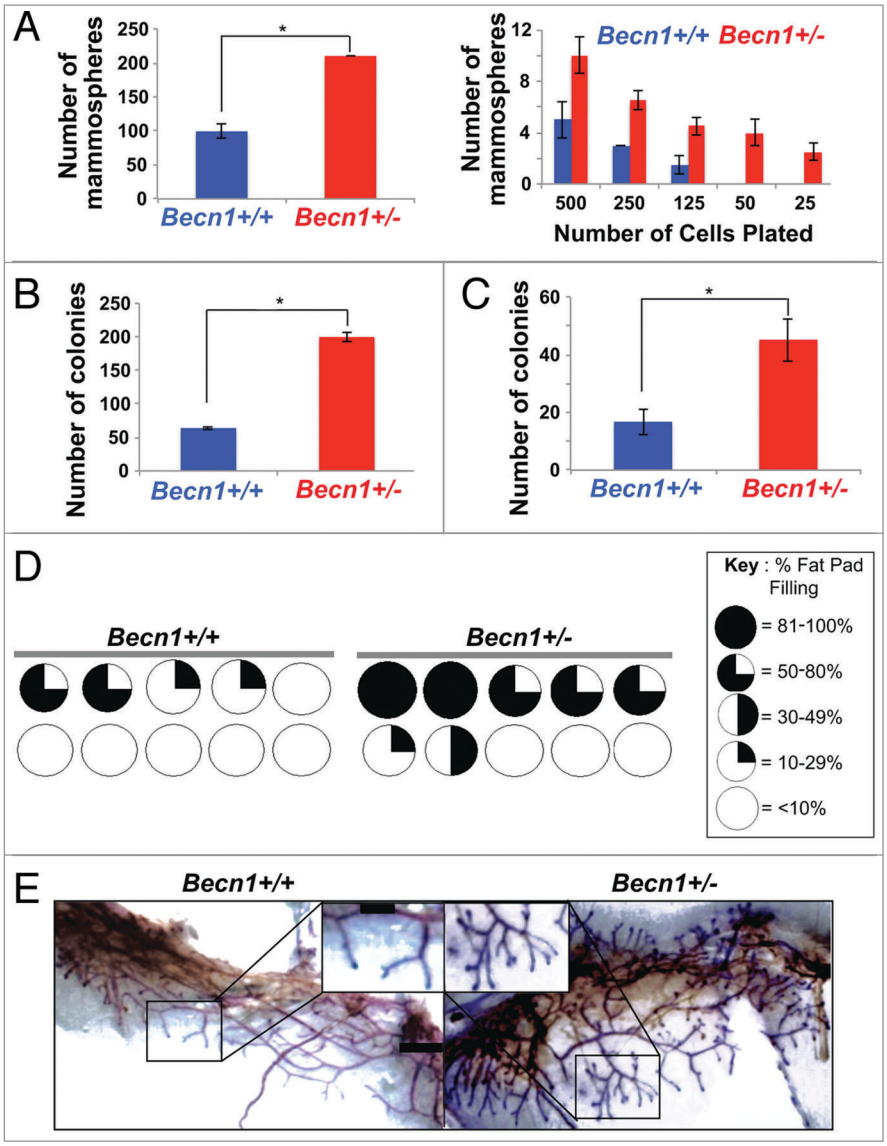

Figure 3. Monoallelic *Becn1* loss results in functionally enriched mammary stem and progenitor cell populations. (**A–C**) Freshly isolated *Becn1*$^{+/+}$ (blue) and *Becn1*$^{+/-}$ (red) MECs were used, experiments were performed 3 independent times and outcomes are presented as means ± SDs. (**A**) Primary mammosphere assays performed using Pi^{-} LIN(CD31,CD45,LY76)$^{-}$ CD24^{+} CD29^{hi} MECs plated at 20,000 cells per well (left) and in limiting dilution of 500 to 25 CD24^{+} CD29^{hi} MECs plated (right) reveal increased MaSC activity in *Becn1*$^{+/-}$ MECs. (**B**) 3D colony-formation by CD24^{+} CD29^{hi} *Becn1*$^{+/-}$ compared with *Becn1*$^{+/+}$ MECs plated at 20,000 cells per well shows increased MaSC activity. (**C**) Colony formation by CD24^{+} CD29^{lo} *Becn1*$^{+/-}$ compared with *Becn1*$^{+/+}$ MECs plated at 1,000 cells per well reveals increased colony forming ability in 2D-matrigel conditions. (**D**) Increased repopulation frequency and mammary fat pad filling are seen following transplantation of 250 CD24^{+} CD29^{hi} *Becn1*$^{+/-}$ MECs isolated from 5-wk-old mice. *Becn1*$^{+/+}$ (left) and *Becn1*$^{+/-}$ (right), contralateral transplantations in wild-type recipient mouse. Circles represent fat pads and the black color represents the percentage of the mammary fat pad that is filled in. (**E**) Representative whole mount images of outgrowths from contralateral CD24^{+} CD29^{hi} *Becn1*$^{+/+}$ and *Becn1*$^{+/-}$ MEC transplantation are shown and reveal increased ductal side branching in *Becn1*$^{+/-}$ samples. *$P < 0.05$ by a 2-tailed Student *t* test. Scale bar: (**E**) 5 mm for whole mounts; 2 mm for whole mount enlargements.

Monoallelic *Becn1* loss results in TNFRSF11A-NFKB pathway activation in mammary tissues

TNFSF11/TNF11/RANKL (tumor necrosis factor [ligand] superfamily, member 11) has been implicated in progesterone-

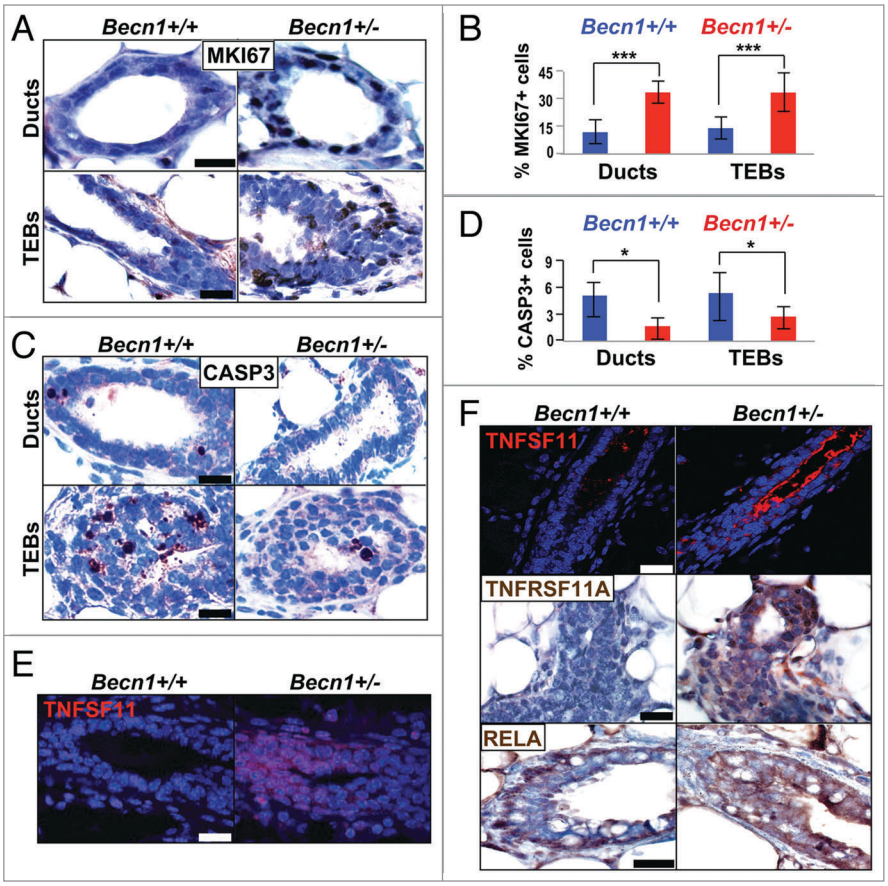

Figure 4. Outgrowths from CD24$^+$ CD29^{hi} *Becn1*$^{+/-}$ MEC transplantation display increased proliferation and TNFSF-NFKB pathway activation. (**A–D, and F**) Examination of outgrowths from contralateral transplantations of CD24$^+$ CD29^{hi} *Becn1*$^{+/+}$ and *Becn1*$^{+/-}$ MECs, and (**E**) native MGs from 6.5-wk-old cohoused *Becn1*$^{+/+}$ and *Becn1*$^{+/-}$ littermates. (**A**) Representative images show more MKI67$^+$ cells in ducts (top) and TEBs (bottom) of outgrowths from CD24$^+$ CD29^{hi} *Becn1*$^{+/-}$ MEC transplantation; (**B**) quantification of MKI67$^+$ cells in mammary ducts and TEBs is shown as means ± SDs (n = 3 mammary gland specimens per genotype). (**C**) Representative images show fewer cleaved CASP3-staining cells in ducts (top) and TEBs (bottom) of outgrowths from CD24$^+$ CD29^{hi} *Becn1*$^{+/-}$ MEC transplantation; (**D**) quantification of cleaved CASP3$^+$ cells in mammary ducts and TEBs is shown as means ± SDs (n = 3 mammary gland specimens per genotype). Increased TNFSF11 (red) expression is seen in (**E**) native MGs from 6.5-wk-old *Becn1*$^{+/-}$ mice and (**F**) outgrowths from contralateral CD24$^+$ CD29^{hi} *Becn1*$^{+/-}$ MEC transplantation (top panel). Increased TNFRSF11A (middle panel) and RELA (bottom panel) levels are also seen in outgrowths from CD24$^+$ CD29^{hi} *Becn1*$^{+/-}$ MEC transplantation. Scale bar: (**A, C, E, and F**, middle and bottom panels) 30 μm ; (**F**, top panel) 40 μm.

induced MaSC expansion[28] and mice overexpressing TNFSF11 or its receptor, TNFRSF11A/RANK (tumor necrosis factor receptor superfamily, member 11a, NFKB activator), under the mouse mammary tumor virus (MMTV) promoter,[29,30] exhibit mammary phenotypes similar to *Becn1*$^{+/-}$ mice, including excessive ductal side-branching (**Fig. 2**), increased proliferation (**Fig. S1A and S1B**), and mammary hyperplasias (**Fig. 2C**), but no mammary tumors in nulliparous mice.[4,15] We hypothesized that ectopic TNFRSF11A-TNFSF11 signaling may be mediating the increased mammary stem and progenitor cell activities in MGs from *Becn1*$^{+/-}$ mice. TNFSF11 was indeed detected in MGs from pubertal *Becn1*$^{+/-}$ mice (**Fig. 4E**) and robustly in outgrowths from CD24$^+$ CD29^{hi} *Becn1*$^{+/-}$ MEC transplantations (**Fig. 4F**). Consistent with aberrant TNFRSF11A pathway activation, outgrowths from CD24$^+$ CD29^{hi} *Becn1*$^{+/-}$ MEC transplantation also displayed increased TNFRSF11A expression (**Fig. 4F**) and likely activation of the downstream effector NFKB axis,[31] as indicated by increased expression, though not apparent nuclear localization, of RELA (**Fig. 4F**). In agreement with previous studies,[28-30,32-34] this data suggests that aberrant TNFRSF11A pathway activation may play a role in the MaSC and progenitor cell expansion observed in association with monoallelic *Becn1* loss. However, further studies will need to be conducted to determine whether TNFRSF11A signaling is responsible for the mammary phenotypes observed in *Becn1*$^{+/-}$ mice.

Locally increased progesterone signaling in MGs from *Becn1*$^{+/-}$ mice

Given that progesterone is required for mammary ductal side-branching[35] and TNFSF11 is a mediator of both progesterone signaling[28,32] and progestin-induced mammary tumorigenesis,[34] we examined MGs from cohoused *Becn1*$^{+/+}$ and *Becn1*$^{+/-}$ littermate mice for evidence of progesterone signaling. As shown (**Fig. 5A and B**), monoallelic *Becn1* loss resulted in higher proportion of PGR (progesterone receptor)-positive MECs. Transplantation of CD24$^+$ CD29^{hi} *Becn1*$^{+/+}$ and *Becn1*$^{+/-}$ MECs into contralateral fat pads of a wild-type recipient resulted in mammary outgrowths of both *Becn1* genotypes in the same mouse; similar to native MGs, and despite uniform systemic hormone levels, the proportion of nuclear PGR-positive cells was again higher in outgrowths generated by *Becn1*$^{+/-}$ MECs (**Fig. 5C and D**), indicating that monoallelic *Becn1* loss results in locally-regulated increased progesterone signaling.

To investigate the role of hormonal signaling in the mammary hyper side-branching phenotype observed in association with monoallelic *Becn1* loss, *Becn1*$^{+/+}$ and *Becn1*$^{+/-}$ mice were ovariectomized at 3 to 4 wk of age. In the absence of endogenous hormone production, MGs from *Becn1*$^{+/+}$ and *Becn1*$^{+/-}$ mice displayed similar ductal side-branching (**Fig. 5E**), whereas hormonal stimulation of ovariectomized mice with exogenous 17β-estradiol and progesterone[32] rescued the hyper ductal side-branching phenotype in *Becn1*$^{+/-}$ vs. *Becn1*$^{+/+}$ mice (**Fig. 5E**). This data implies that hormonal signaling is required for the increased ductal side-branching seen in MGs from *Becn1*$^{+/-}$ mice, and supports our observations that this phenotype is

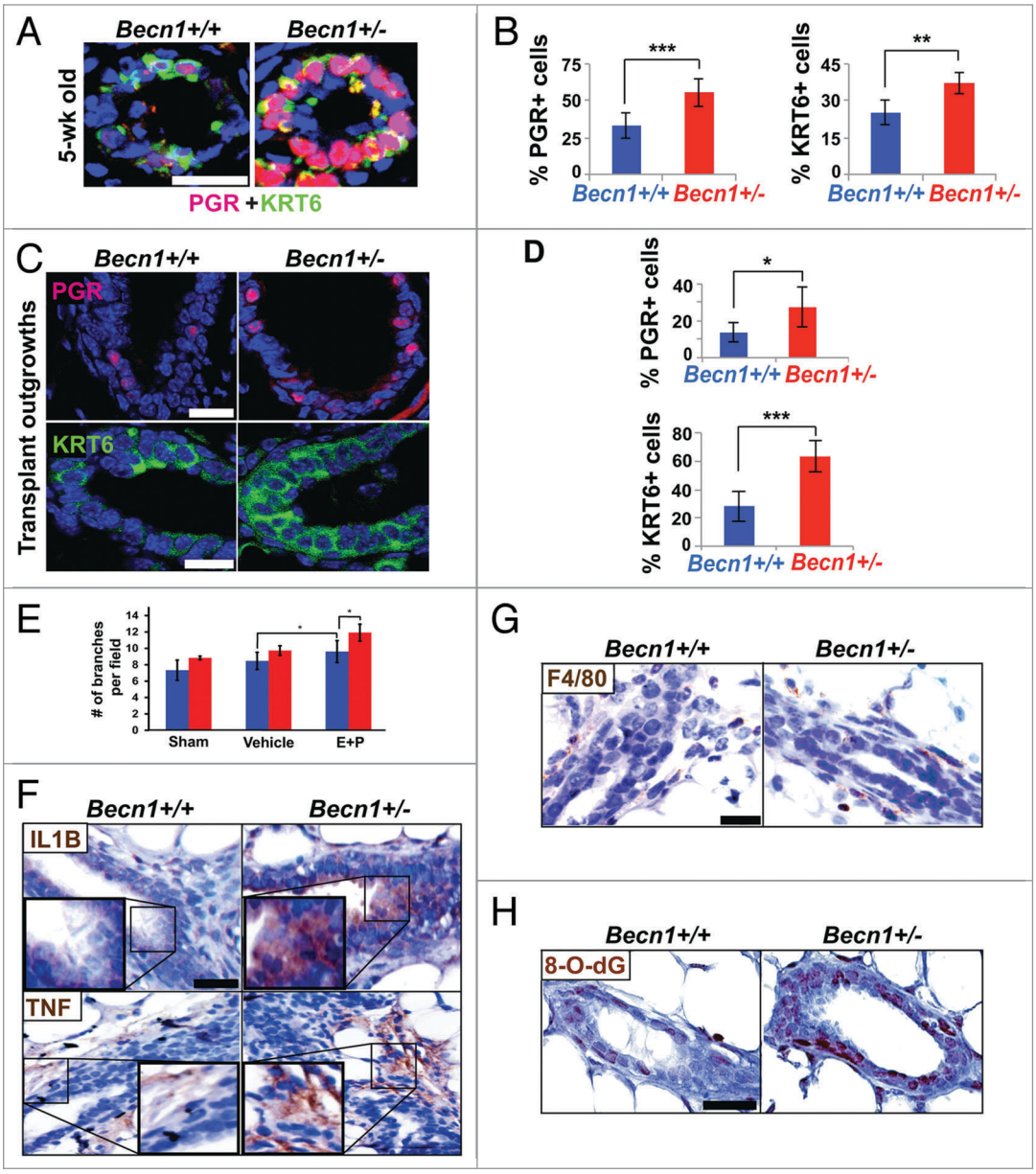

Figure 5. Augmented progesterone signaling, cytokines, and oxidative stress detected upon monoallelic *Becn1* loss. (**A and C**) Nuclear PGR (red) and KRT6 (green) cell staining in native MGs from cohoused *Becn1*$^{+/+}$ and *Becn1*$^{+/-}$ MEC and outgrowths from contralateral CD24^{+} CD29^{hi} *Becn1*$^{+/+}$ and *Becn1*$^{+/-}$ MEC transplantation. (**A**) Representative images of PGR^{+} and KRT6^{+} cells and (**B**) quantification of nuclear PGR^{+} cells (left) and KRT6^{+} cells (right) in MGs from 5-wk old mice reveals increased numbers of PGR^{+} and KRT6^{+} cells in *Becn1*$^{+/-}$ mice. (**C**) Representative images of nuclear PGR^{+} cells (top panel) and KRT6^{+} cells (bottom panel) in outgrowths from contralateral CD24^{+} CD29^{hi} *Becn1*$^{+/+}$ and *Becn1*$^{+/-}$ MEC transplantation with (**D**) quantification of PGR^{+} cells (top panel) and KRT6^{+} cells (bottom panel). Results are presented as means ± SDs (n = 3 mammary gland specimens per genotype). (**E**) Quantification of ductal side-branching in MGs from hormonally stimulated following ovariectomization, where Sham = ovariectomized, Vehicle = ovariectomized + 100 μL sesame oil daily, and E + *P* = ovariectomized + 5 μg 17B-estradiol + 5 mg progesterone in 100 μL of sesame oil daily. (**F–H**) Examination of outgrowths from contralateral transplantations of CD24^{+} CD29^{hi} *Becn1*$^{+/+}$ and *Becn1*$^{+/-}$ MECs. (**F**) Increased IL1B (top panel) and TNF (bottom panel) seen in outgrowths from *Becn1*$^{+/-}$ MEC transplantation. (**G**) Similar F4/80 staining detected in outgrowths from *Becn1*$^{+/+}$ and *Becn1*$^{+/-}$ MEC transplantation. (**H**) Increased 8-O-dG is seen in outgrowths from *Becn1*$^{+/-}$ MEC transplantation. *$P < 0.05$, **$P < 0.01$, and ***$P < 0.001$ by a 2-tailed Student *t* test. Scale bar: (**A, C, F, G, and H**) 30 μm; (**E**) 50 μm.

associated with progesterone axis activation (**Fig. 2C and D**) and is likely hormonally regulated.

In progesterone-driven TNFRSF11A signaling, exogenous progesterone activates PGR-positive MECs to secrete TNFSF11, which in turn induces proliferation of neighboring TNFRSF11A-expressing mammary stem and progenitor cells and subsequent generation of more PGR-positive MECs, thus creating a positive feedback loop.[28,32] In macrophages, TNFSF11 production and activation of TNFRSF11A-NFKB signaling is driven by proinflammatory cytokines.[36] In our studies, where contralaterally transplanted *Becn1*$^{+/+}$ and *Becn1*$^{+/-}$ MECs are exposed to the same systemic hormones, outgrowths generated by CD24^{+} CD29^{hi} *Becn1*$^{+/-}$ MECs displayed increased IL1B (interleukin 1, β) and TNF/TNFα (tumor necrosis factor) levels (**Fig. 5F**), which were not accompanied by enhanced macrophage infiltration (**Fig. 5G**). Together these studies indicate that IL1B and TNF were likely secreted by and acting autonomously on *Becn1*$^{+/-}$ MECs.

Autophagy-deficient tissues commonly harbor a proinflammatory microenvironment,[37] mainly attributed to increased reactive oxygen species (ROS) due to impaired removal of damaged mitochondria.[37] Consistent with their functional autophagy defect (**Fig. S2E and S2F**), CD24^{+} CD29^{hi} *Becn1*$^{+/-}$ MEC-generated

outgrowths exhibited increased oxidative stress, as evaluated by 8-oxo-7,8-dihydroguanine (8-O-dG) staining (**Fig. 5H**).

Becn1$^{+/-}$ mice develop spontaneous mammary tumors following parity

In earlier studies which reported mammary hyperplasias, but no mammary tumors, in *Becn1*$^{+/-}$ mice independent of age and parity,[4,15] the mouse genetic background was C57BL/6, which is known to suppress mammary tumorigenesis.[38] To ensure that mammary tumor studies in *Becn1*$^{+/-}$ mice were not confounded by the C57BL/6 status, we changed the genetic background of *Becn1*$^{+/-}$ mice[5] to FVB/N, which is more amenable to mammary tumorigenesis studies.[38]

Nulliparous and multiparous (post 2 pregnancy/lactation/involution cycles) *Becn1*$^{+/+}$ and *Becn1*$^{+/-}$ female mouse cohorts were generated, cohoused and monitored for mammary tumor formation. Similar to C57BL/6 mice,[4,15] both nulliparous and multiparous *Becn1*$^{+/-}$ FVB/N mice developed lymphomas, lung and liver tumors, and mammary hyperplasias with age. Furthermore, mammary ducts from older (24-mo-old) nulliparous *Becn1*$^{+/-}$ FVB/N mice showed increased cellular density and irregular epithelial cell layering (**Fig. 6A**). Similar, but more pronounced, changes of increased epithelial density and disorganized ductal architecture were observed in MGs from multiparous *Becn1*$^{+/-}$ multiparous mice at a younger age (14 to 17 mo) (**Fig. 6B**). In contrast to C57BL/6 mice and nulliparous FVB/N mice, 4 out of 21 mice (19%) of multiparous *Becn1*$^{+/-}$ female mice developed mammary tumors between the ages of 14 and 24 mo (**Fig. 6C**). Tumor #1 displayed squamous and focal glandular differentiation, with keratinizing differentiated squamous and nonkeratinized poorly differentiated regions. Tumor #2 displayed well-differentiated keratinizing squamous differentiation with foci of basaloid squamous and glandular components; both tumors #1 and 2 showed pervasive KRT6- and KRT14-positivity, but no PGR staining. Tumor #3 had characteristics of glandular differentiation with small foci of well-differentiated keratinizing squamous component, and was positive for KRT6 and KRT14, but not PGR. Tumors #1–3 were characterized as invasive adenosquamous carcinomas, a type of metaplastic carcinoma seen in the mammary gland. Tumor #4 displayed a marked cribriform pattern and luminal eosinophilic cylinders resembling the invasive mammary tumor known as an adenoid cystic carcinoma, and was KRT6-negative, but PGR-positive. Despite diversity in histology likely due to tumor heterogeneity,[39] most tumors were squamous, KRT6-positive, and basal-like (KRT14-positive) and all showed negative correlation between KRT6 and PGR expression.

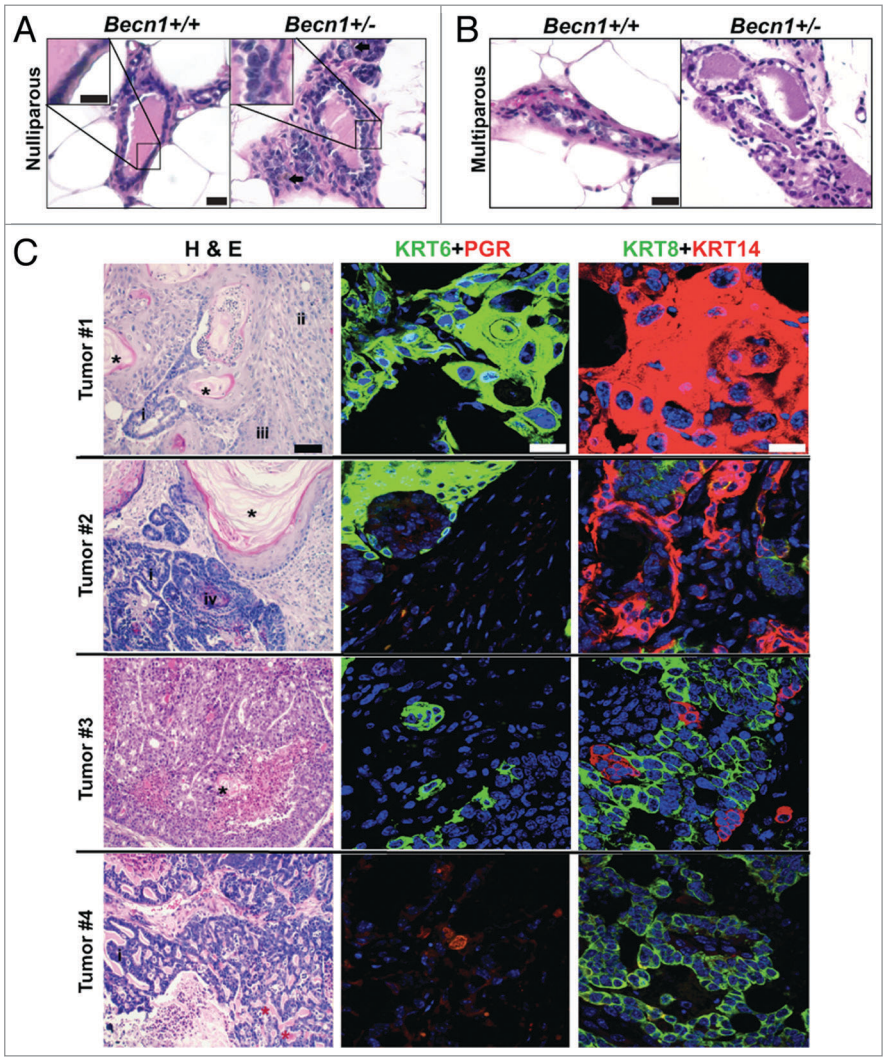

Figure 6. Spontaneously arising mammary tumors are detected in multiparous *Becn1*$^{+/-}$ FVB/N mice. (**A and B**) Hematoxylin and eosin staining (H&E) of MG sections from *Becn1*$^{+/+}$ (left) and *Becn1*$^{+/-}$ (right) FVB/N mice: (**A**) Representative images from MGs of nulliparous 21- to 22-mo-old mice reveals increased epithelial cell density and inflammatory cell infiltration (brown, identified with arrow) in *Becn1*$^{+/-}$ mice. (**B**) Representative H&E images of MGs from parous 14- to 17-mo-old mice reveals increased epithelial cell density and disorganized cell layering in MGs from *Becn1*$^{+/-}$ mice. (**C**) Representative images from 4 spontaneously arising mammary tumors in parous *Becn1*$^{+/-}$ FVB/N mice (Tumors #1 to 4). Left panels are representative H&Es; middle panels, KRT6 (green) and nuclear PGR (red) staining; and right panels, KRT8 (green) and KRT14 (red) staining. (*) and (*) denote keratin pearls and basement membrane/eosinophilic hyaline materials, respectively. Tumor type denotations are identified by: (i) for glandular components, (ii) for poorly to moderately differentiated squamous cell carcinoma, (iii) for well-differentiated squamous cell carcinoma, and (iv) for basaloid squamous cell carcinoma. Scale bar: (**A and B**) 30 μm and KRT8 and KRT14 (**C**); (**C**) 200 μm for H&Es; (**C**) 50 μm for KRT6 and PGR.

Monoallelic *Becn1* loss accelerates WNT1-driven mammary tumorigenesis

Given our findings that monoallelic *Becn1* loss promotes KRT6-positive immature mammary cell accumulation (**Fig. 1**), we investigated whether *Becn1* heterozygosity has an impact on mammary tumorigenesis in the context of oncogenic WNT1 activation, where KRT6-positive bipotent MaPCs are considered tumor-initiating cells.[18,20]

As shown (**Fig. 7A**; **Fig. S5A**), *Becn1*$^{+/-}$;MMTV-*Wnt1* mice displayed significantly shorter mammary tumor-free survival (4 vs. 7.2 mo; P 0.004) and overall survival (4.7 vs. 7.5 mo; $P < 0.001$) compared with *Becn1*$^{+/+}$;MMTV-*Wnt1* mice. Consistent with defective autophagy status, mammary tumors from *Becn1*$^{+/-}$;MMTV-*Wnt1* mice showed reduced LC3B levels and SQSTM1 aggregates (**Fig. S5B**). Tumors arising in *Becn1*$^{+/+}$;MMTV-*Wnt1* mice displayed known characteristics of MMTV-*Wnt1* mammary tumors,[40] as they were KRT6-positive adenosquamous carcinomas with high KRT8 and low KRT14 levels, and variable ESR (estrogen receptor) and PGR expression (**Fig. 7B**). Mammary tumors from *Becn1*$^{+/-}$;MMTV-*Wnt1* mice were also mostly adenosquamous carcinomas, but exhibited higher KRT6 levels, were more basal-like, as KRT14 expression was very prominent, and did not express ER or PGR (**Fig. 7B**). Furthermore, while proliferation was similar, apoptosis was suppressed in tumors from *Becn1*$^{+/-}$;MMTV-*Wnt1* mice (**Fig. S5C and S5D**).

Gene expression profiling also showed that mammary tumors from *Becn1*$^{+/-}$;MMTV-*Wnt1* mice showed higher expression of KRT6 and other basal keratins, including KRT5, KRT14, and KRT17; they also displayed CTNNB1/β-catenin (catenin [cadherin-associated protein], β 1, 88 kDa) upregulation (**Fig. 7C**), indicating that monoallelic *Becn1* loss rendered WNT1-induced mammary tumors basal-like and further enhanced CTNNB1 signaling already present due to WNT1 activation. An earlier publication reported that TP53 expression is regulated by BECN1 and, as such, may contribute to BECN1-associated tumor suppression.[41] In our studies, mammary tumors from *Becn1*$^{+/+}$;MMTV-*Wnt1* and *Becn1*$^{+/-}$;MMTV-*Wnt1* mice did not exhibit differences in expression of TP53 transcriptional

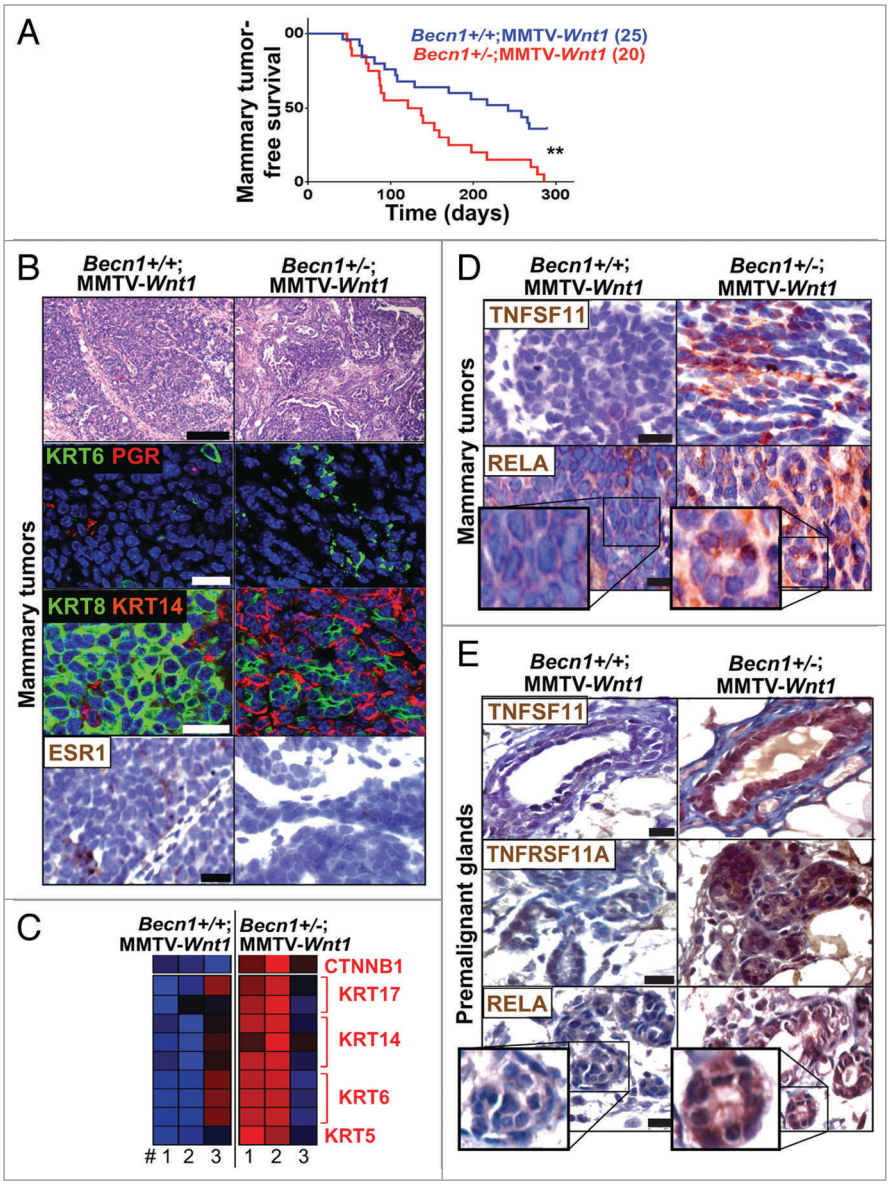

Figure 7. Monoallelic *Becn1* loss accelerates WNT1-driven tumorigenesis and gives rise to mammary tumors with TNFRSF11A-NFKB1 pathway activation and basal-like characteristics. Basal-like characteristics and TNFRSF11A-NFKB1 signaling activation are detected in spontaneous mammary tumors that arise faster in *Becn1*$^{+/-}$;MMTV-*Wnt1* (right) compared with *Becn1*$^{+/+}$;MMTV-*Wnt1* mice (left). (**A**) Kaplan-Meier curves for mammary tumor-free survival in *Becn1*$^{+/+}$;MMTV-*Wnt1* (n = 25) and *Becn1*$^{+/-}$;MMTV-*Wnt1* (n = 20) mice demonstrates decreased mammary tumor-free survival in *Becn1*$^{+/-}$;MMTV-*Wnt1* mice. (**B–E**) Examination of mammary tumors and premalignant MGs from *Becn1*$^{+/+}$;MMTV-*Wnt1* (left) and *Becn1*$^{+/-}$;MMTV-*Wnt1* (right) mice. (**B**) Representative images of H&E staining (top panel), KRT6 (green) and nuclear PGR (red) cell staining (second panel), KRT8 (green) and KRT14 (red) cell staining (third panel), and nuclear ESR1 staining (bottom panel) on tumor sections. (**C**) Heat map representation of microarray analysis confirms basal-like tumor characteristics along with higher CTNNB1 expression in tumors from *Becn1*$^{+/-}$;MMTV-*Wnt1* mice. Statistical significance of upregulation of a given signature on a group of samples was determined using a Fischer exact test for enrichment of samples with significant ($P < 0.05$) signature expression in the group relative to samples outside the group. (**D**) Representative images of TNFSF11 (top panel) and RELA (bottom panel) expression in mammary tumors, and (**E**) TNFSF11 (top panel), TNFRSF11A (center panel), and RELA (bottom panel) expression in premalignant MGs from 6- to 10-wk-old cohoused *Becn1*$^{+/+}$;MMTV-*Wnt1* and *Becn1*$^{+/-}$;MMTV-*Wnt1* littermates. $P < 0.01$ determined by a Mantel-Cox test for Kaplan-Meier curves. Scale bar: (**B**) 200 μm for H&Es; (**B, D, and E**) 30 μm for all other panels.

target genes (data not shown), thus suggesting that in the context of WNT1-driven mammary tumorigenesis, differential TP53 activation is not a likely contributor to mammary tumor acceleration in association with monoallelic *Becn1* loss.

Consistent with our finding that monoallelic *Becn1* loss results in increased mammary stem and progenitor cell activity in association with TNFRSF11A-NFKB pathway activation (**Figs. 1**, **3**, **and 4**), tumors from *Becn1*$^{+/-}$; MMTV-*Wnt1* mice exhibited increased TNFSF11 expression and nuclear RELA staining (**Fig. 7D**). Premalignant MGs from *Becn1*$^{+/-}$;MMTV-*Wnt1* mice displayed even higher TNFSF11, TNFRSF11A, and nuclear RELA levels (**Fig. 7E**), indicating that early activation of TNFRSF11A-NFKB signaling may contribute to promotion of WNT1-driven mammary tumorigenesis by monoallelic *Becn1* deletion. However, additional studies must be conducted to further investigate whether aberrant TNFRSF11A pathway activation is responsible for the accelerated mammary tumor development in *Becn1*$^{+/-}$;MMTV-*Wnt1* mice.

Human breast cancers with low *BECN1* mRNA expression and an activated WNT pathway gene signature have poor prognosis

To examine the clinical relevance of our mouse tumor studies, we identified human breast cancers exhibiting a gene signature consistent with WNT pathway activation and stratified them for high vs. low (above or below the mean across samples, respectively) expression of *BECN1* mRNA. In 2 independent breast cancer cohorts,[42,43] tumors with low *BECN1* expression and an activated WNT pathway gene signature had significantly worse prognosis than tumors with high *BECN1* mRNA and WNT pathway activation (**Fig. 8A and B**) and also correlated with the triple negative breast cancer (TNBC) subtype (**Fig. 8C and D**). In a cohort excluding ERBB2-positive cancers,[42] tumors with low *BECN1* expression and an activated WNT pathway gene signature were almost exclusively TNBCs and showed TNFRSF11A pathway activation (**Fig. 8D**), similar to mammary tumors from *Becn1*$^{+/-}$;MMTV-*Wnt1* mice (**Fig. 7C**).

In the Sabatier data set,[43] within low *BECN1*-expressing tumors, an activated WNT pathway gene signature conferred worse disease-free survival (DFS), whereas in high *BECN1*-expressing tumors, it was associated with improved DFS (**Fig. S6A**). In tumors not displaying WNT pathway activation, *BECN1* expression did not affect DFS (**Fig. S6A**). In the Hatzis, ERBB2-negative breast tumor database, in low *BECN1*-expressing and mostly triple-negative tumors, WNT pathway activation did not have an impact on DFS, whereas in high *BECN1*-expressing tumors, it was again associated with improved DFS (**Fig. S6B**). In tumors not displaying upregulation of a WNT pathway gene signature, low *BECN1* expression conferred worse DFS (**Fig. 6B**). Examination of additional breast cancer databases and prospective evaluation of clinically annotated breast tumor biopsies will be necessary to further define how the combination of low *BECN1* expression and WNT pathway activation affects prognosis within the different breast cancer subtypes.

Discussion

Role of *Becn1* in the homeostasis of the mammary cell hierarchy

Our studies identify monoallelic *Becn1* loss as a potential contributor to immature MEC expansion and, thus, deregulation of the mammary cell hierarchy. Our findings come at a time of great interest in the role of autophagy in stem and progenitor cell biology. Recent studies show that autophagy supports stem cell survival in the hematopoietic[44] and nervous[45] systems, and in the context of an ERα-positive and an ERBB2-positive breast cancer cell lines.[10] Here we report that partial *Becn1* deficiency leads to increased mammary stem and progenitor cell activities, and we hypothesize that this contributes to increased mammary tumorigenesis in association with monoallelic *Becn1* loss under conditions of further mammary stem and progenitor pool expansion due to either parity or activation of particular oncogenes, such as WNT1. Our work identifies 2 specific contexts in which *Becn1* heterozygosity promotes mammary tumorigenesis, and provides insight into the seemingly paradoxical roles of BECN1, and autophagy in general, as both tumor-suppressive and tumor-promoting functions. Furthermore, our studies suggest that low *BECN1* expression has an impact on tumor histology in the case of WNT1-driven tumorigenesis, giving rise to tumors with more basal and TNBC characteristics.

An important question that arises from this work and the focus of future studies is whether the *Becn1* heterozygosity-associated mammary phenotypes described in our study are secondary to nonautophagy-related roles of BECN1 in mammary development and tumorigenesis. Although the impact of conditional *Atg7* deficiency on mammary tumor formation following parity or WNT1 activation has not yet been explored, it is intriguing that biallelic *Atg7* deletion delays mammary fat pad filling during puberty and does not result in the hyper side-branching phenotype observed in *Becn1*$^{+/-}$ mice, pointing to a BECN1-specific, and unrelated to autophagy, role in ductal morphogenesis. Alternatively, an autophagy dosage effect on mammary hierarchy may contribute to the observed phenotypes. In that respect, a more severe autophagy defect, such as that conferred by biallelic *Atg7* loss, may drastically compromise MaSC and progenitor cell survival, and possibly suppress tumorigenesis, whereas partially deficient autophagy due to *Becn1* heterozygosity may result in "injured," but still surviving, mammary stem and progenitor cells with increased proliferation, which may promote tumor development under conditions that further deregulate the homeostasis of mammary cell hierarchy; an autophagy dosage effect on mammary differentiation and possibly tumorigenesis would be consistent with the results of recent studies on the role of autophagy inhibition in lung cancer.[11]

Monoallelic *Becn1* loss and TNFRSF11A-NFKB signaling activation in mammary tissues

Our studies demonstrate that MGs from pubertal and adult *Becn1*$^{+/-}$ mice exhibit excessive ductal side-branching in association with abnormal TNFSF11 expression and TNFRSF11A-NFKB axis activation. TNFSF11 is a member of the tumor

necrosis factor (TNF) ligand superfamily, primarily known for its role in bone remodeling and metastasis[33] and also implicated in MaPC expansion and progestin-induced tumorigenesis.[34,46] High TNFRSF11A and TNFSF11 levels were also reported in breast cancers lacking ESR1 and PGR expression and in high-grade and highly proliferative breast tumors;[47] consistent with these results, we also found evidence of TNFRSF11A pathway activation in aggressive basal-like tumors exhibiting low *BECN1* expression and an activated WNT pathway gene signature. Furthermore, TNFRSF11A overexpression in breast cancer cell lines has been reported to disrupt mammary cell fate, induce epithelial-to-mesenchymal transition (EMT) and promote mammary tumorigenesis and metastasis.[47] In our studies, tumors originating in both *Becn1*$^{+/+}$;MMTV-*Wnt1* and *Becn1*$^{+/-}$;MMTV-*Wnt1* mice retained epithelial keratin expression, and neither expressed mesenchymal markers, such as VIM/vimentin (data not shown) nor gave rise to visible metastases at the time of necropsy. However, since metastatic lesions are not usually noted in MMTV-*Wnt1* mice sacrificed when their primary mammary tumors reach experimental endpoints,[40] specifically designed metastasis studies, involving mammary tumor resection survival surgery and/or intracardial injection of tumor-derived mammary tumor cell lines, will be necessary to determine the role of BECN1 in metastasis and EMT in the context of WNT pathway activation.

Our findings, together with the striking similarities in mammary development and tumor phenotypes between *Becn1*$^{+/-}$ and MMTV-*Tnfrsf11a* (or MMTV-*Tnfsf11*) mice, suggest that the TNFRSF11A pathway may mediate the impact of monoallelic *Becn1* loss on mammary cell hierarchy, morphogenesis and tumorigenesis. However, whether ectopic TNFRSF11A pathway activation is responsible for, or contributes to, MaSC and progenitor expansion and increased tumor susceptibility following parity or WNT pathway activation upon monoallelic *Becn1* loss requires further mechanistic investigation.

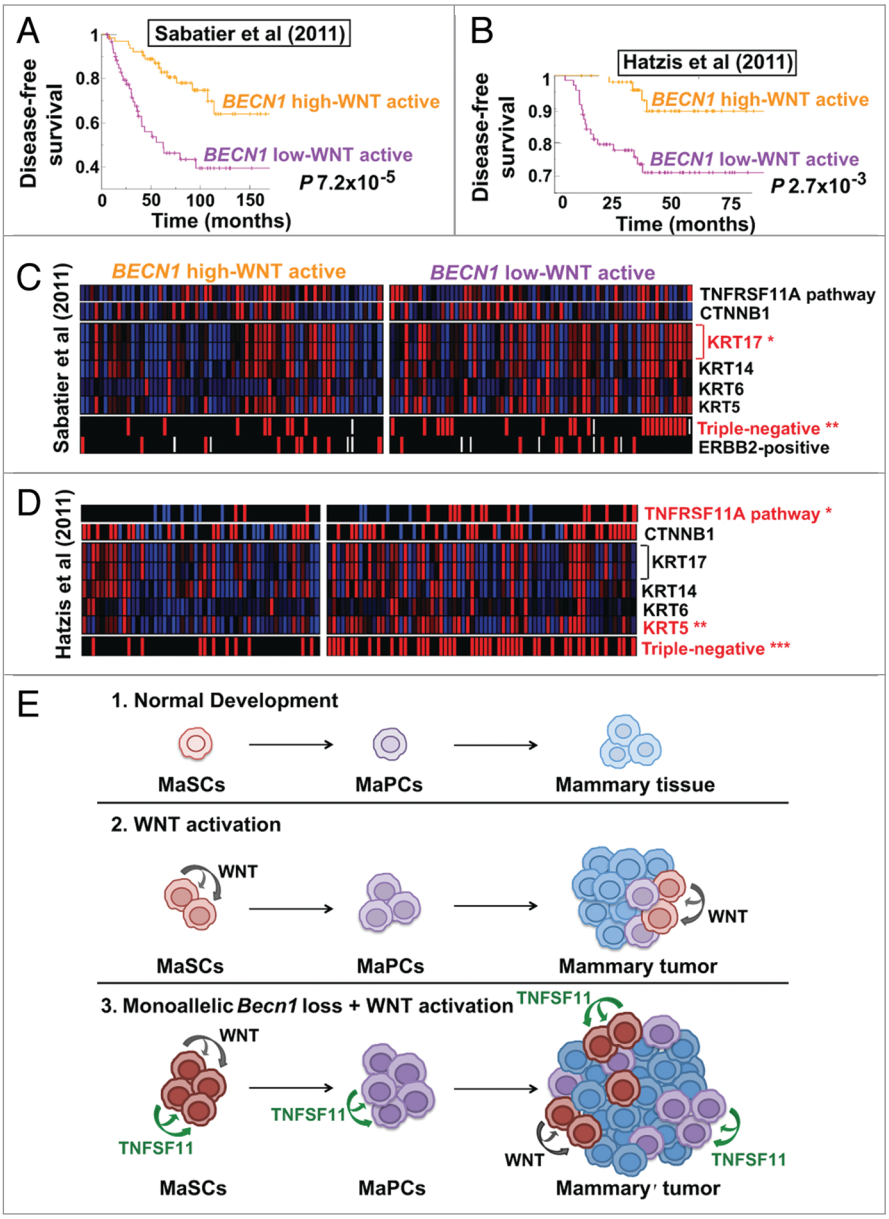

Figure 8. Human breast cancers with low *BECN1* expression and an activated WNT pathway gene signature have poor prognosis. (**A–D**) Kaplan-Meier curves and GSEA for breast tumors displaying an activated WNT pathway gene signature and stratified for *BECN1* expression (see Methods). (**A**) Disease-free survival for patients with breast cancers annotated in the Sabatier cohort (P 7.2 × 10^{-5}). (**B**) Disease-free survival for patients with ERBB2-negative breast cancers annotated in the Hatzis cohort (P 2.7 × 10^{-3}). Gene expression analysis comparison in (**C**) the Sabatier cohort and (**D**) the Hatzis cohort reveals that breast cancers with low *BECN1* and an activated WNT pathway gene signature are primarily triple-negative, have basal-like characteristics, and display TNFRSF11A pathway activation and higher CTNNB1. P values were calculated by the Fischer exact test (see Materials and Methods). (**E**) Model for the cooperation between monoallelic *BECN1* loss and WNT pathway activation in mammary tumorigenesis. *$P < 0.05$, **$P < 0.01$, ***$P < 0.001$.

Which cell type produces TNFSF11 in MGs from *Becn1*$^{+/-}$ mice is another topic of interest. TNFSF11 production by MECs is primarily considered the result of progesterone stimulation,[28,32] whereas in macrophages, adipocytes, and breast cancer cells, proinflammatory cytokines can also upregulate TNFSF11.[36,48,49] Our transplantation studies argue in support of TNFSF11 production by MECs in response to proinflammatory cytokine release by MECs themselves: (1) mammary outgrowths were exposed to same systemic progesterone levels, as CD24^{+} CD29^{hi} *Becn1*$^{+/+}$ and *Becn1*$^{+/-}$ MECs were transplanted in contralateral fat pads of recipient mice. Increased

progesterone signaling in association with monoallelic *Becn1* loss must therefore result from a locally-induced expansion of PGR-expressing cells; (2) 2 proinflammatory cytokines known to induce TNFSF11 production, namely IL1B and TNF, were detected in $CD24^{+}$ $CD29^{hi}$ $Becn1^{+/-}$ MEC-generated outgrowths; (3) $CD24^{+}$ $CD29^{hi}$ $Becn1^{+/+}$ and $Becn1^{+/-}$ MEC transplantations were performed in wild-type recipient mice, thus all stromal cells were wild type. The fact that, similar to MGs from $Becn1^{+/-}$ mice, outgrowths from $CD24^{+}$ $CD29^{hi}$ $Becn1^{+/-}$ MEC transplantation also exhibited increased ductal side-branching and TNFSF11 production indicate that MECs are sufficient to induce these mammary phenotypes. Furthermore, macrophage infiltration was similar in $CD24^{+}$ $CD29^{hi}$ $Becn1^{+/+}$ and $Becn1^{+/-}$ MEC-generated outgrowths; (4) increased oxidative stress, a inducer of proinflammatory cytokine production,[37] was documented in $CD24^{+}$ $CD29^{hi}$ $Becn1^{+/-}$ MEC-generated outgrowths; (5) autophagy-deficient status, commonly associated with inflammation and cytokine release,[14,37] was maintained in $CD24^{+}$ $CD29^{hi}$ $Becn1^{+/-}$ MEC-generated outgrowths. This study provides evidence for an essential role of BECN1 in restricting mammary stem and progenitor cell expansion and limiting ectopic TNFRSF11A pathway activation, 2 pathways known to be deregulated in particular contexts of mammary tumorigenesis.[18,30,34]

Shedding light in the complex role of *Becn1* in mammary tumorigenesis

BECN1, and autophagy in general, have complex roles in tumorigenesis: allelic *BECN1* deletions have been reported in human cancers,[2] and $Becn1^{+/-}$[4,5] and other *Atg*-deficient[50,51] mice are tumor-prone, in support of a tumor suppressor role for autophagy in cancer. However, autophagy also preserves tumor cell survival under stress and likely contributes to tumor progression[11] and treatment resistance.[52] While apoptosis-deficient $Becn1^{+/-}$ iMMECs, compared with their wild-type counterparts, result in earlier mammary tumor development in nude mice,[6] monoallelic *Becn1* deletion does not alter ERBB2- or PyMT-driven,[8] while it delays *Palb2* loss-associated,[13] mammary tumorigenesis.

Our studies define specific contexts, either following parity or oncogenic WNT1 activation, in which monoallelic *Becn1* deletion promotes mammary tumorigenesis. Spontaneous tumors arising in $Becn1^{+/-}$ mice after parity display mostly squamous cell characteristics, which is similar to the squamous differentiation seen by Wei and colleagues in lung cancers with low *BECN1* expression.[9] These 2 studies indicate that low *BECN1* expression may drive particular lung and breast cancer subsets toward squamous, rather than adenocarcinoma, histologies, thus also raising the possibility of concurrent EGFR activation.

In the case of WNT pathway activation, we propose that WNT1-driven mammary stem and progenitor cell expansion cooperates with *Becn1* heterozygosity-induced deregulation of the mammary hierarchy to create more transformation-susceptible immature mammary cells (**Fig. 8E**). Since monoallelic *Becn1* loss results in hormone receptor-negative, basal-like mammary tumors, it is possible that corresponding tumor-initiating cells (TICs) reside within the expanded mammary stem and progenitor cell populations,[23] a hypothesis that is worthy of further investigation. If this is the case, other oncogenes deregulating the mammary hierarchy and resulting in expansion of progenitor cell populations may also cooperate with monoallelic *Becn1* loss to promote mammary tumorigenesis.

Low *BECN1* expression and an activated WNT pathway gene signature define a breast cancer subset with poor prognosis

Despite the early discovery that WNT signaling is highly oncogenic in the mammary gland,[18,20] conclusive evidence that it is a tumor-driver in breast cancer lagged behind.[53] In contrast to colorectal tumors, which commonly harbor mutations in canonical WNT pathway genes,[54] breast cancers lack such genetic alterations.[55] However, even in the absence of mutations, canonical WNT pathway activation has been documented in TNBCs by increased CTNNB1 expression and nuclear localization in association with overexpression of the WNT receptor LRP6 (low-density lipoprotein receptor-related protein 6).[56] Also, single nucleotide polymorphisms (SNPs) in WNT pathway genes were associated with ESR1-negative breast cancer risk.[57]

Given (**1**) that monoallelic *Becn1* loss accelerates WNT1-driven mammary tumorigenesis and results in basal-like mammary tumors, and (**2**) the shift in focus from mutational analysis to collective upregulation of WNT signaling in tumors,[58] we interrogated human breast cancer databases for *BECN1* expression and WNT pathway activation, using DNA probes for *BECN1* and a KEGG pathway-annotated gene signature for WNT pathway (hsa04310; http://www.genome.jp/dbget-bin/www_bget?hsa04310). We found that breast tumors with low *BECN1* expression and WNT pathway activation comprise 24–36% of TNBCs and confer poor patient prognosis. Similarities between mammary tumors from $Becn1^{+/-}$;MMTV-*Wnt1* mice and human breast cancers with low *BECN1* levels and WNT pathway activation, i.e. basal-like characteristics, TNFRSF11A pathway activation, and tumor aggressiveness, indicate that our mouse tumor model recapitulates molecular features and outcomes of a sizeable TNBC subgroup. Thus, our mouse model is a unique and clinically relevant preclinical model for a particular subset of breast cancers, and provides a valuable tool to develop useful molecular markers and evaluate targeted approaches for the treatment of these aggressive malignancies. Furthermore, our analysis of human breast cancer gene expression profiling indicates that, rather than genomic BECN1 alterations which may not have an impact on breast tumorigenesis,[16] *BECN1* mRNA expression, which can also be transcriptionally and/or epigenetically regulated, may itself determine breast cancer susceptibility under particular circumstances, such as parity or WNT pathway activation, and thus act as a context-dependent tumor suppressor.

Identifying an aggressive TNBC subtype with low *BECN1* expression and activation of both WNT and TNFRSF11A pathways has the potential to greatly advance targeted breast cancer treatment, given that WNT signaling inhibitors are clinically investigated and a TNFRSF11A pathway inhibitor, denosumab, is already FDA-approved for prevention and treatment of osteoporosis and skeletal-related events in patients with bone-

metastatic solid malignancies.[59] The mechanistic relationship between low *BECN1* expression, an activated WNT pathway gene signature and aberrant TNFRSF11A signaling in breast tumors needs to be further investigated to justify pharmacologic targeting of the TNFRSF11A and/or WNT pathways for treatment of such malignancies. Given our finding that monoallelic *Becn1* loss results in mammary stem and progenitor cell expansion, which may in turn contribute to acceleration of WNT-driven tumorigenesis, it is conceivable that mammary stem and progenitor tumor cells may arise as promising therapeutic targets in the treatment of aggressive breast cancers exhibiting low *BECN1* expression and an activated WNT pathway gene signature.

Altogether our studies identify BECN1 as a mammary tumor suppressor in 2 particular contexts, namely spontaneous mammary tumor formation following parity and WNT1-driven oncogenesis.

Materials and Methods

Mice

For native mammary gland experiments, mice were housed at the Child Health Institute of New Jersey, in pathogen-free facilities, and cared for as per IACUC-approved protocols. For transplantation experiments, recipient mice were housed at Princeton University and procedures were in compliance with IACUC-approved protocols. *Becn1*$^{+/-}$ mice[5] were obtained from Dr S Jin. MMTV-*Wnt1* mice were obtained from Dr Y Li. *Atg7*$^{F/F}$ mice[26] were obtained from Dr Komatsu. *Gfp-Lc3* mice were obtained from Dr Mizushima. *Krt14-Cre* mice[60] were obtained from Jackson Laboratories.

For CD61 analysis and tumor studies, C57BL/6 *Becn1*$^{+/-}$ mice were backcrossed to FVB/N for 10 generations. In vitro MaSC and progenitor cell assays were performed in both C57BL/6 and FVB/N backgrounds. For all other studies involving the *Becn1*$^{+/-}$ genotype, C57BL/6 mice were used. For mammary fat pad filling and ductal side-branching cohoused littermates (for pubertal time points) and cohoused (for at least 3 mo after last pregnancy) multiparous mice were compared. At least 3 animals were compared for each time point. For all immunostaining, littermates or outgrowths from the same recipient mouse were compared. For tumor studies, multiparous mice were cohoused after 2 rounds of pregnancy, nursing, and weaning of their litters. Mice from the multiparous and nulliparous cohorts were palpated weekly for mammary tumor detection. For ovariectomization and stimulation studies procedures were performed as previously described.[32]

Mammosphere and colony-forming assays

Primary mammosphere assays were performed as previously described.[23,25] MaSC viability assays under ultra low attachment were performed as previously described, and mammospheres were counted. 20,000 CD24$^+$ CD29^{hi} MECs per well were plated on ultra-low attachment plates (Costar, 3471) for 10 to 15 d in Dulbecco's modified Eagle's medium (DMEM)/F12, EGF (epidermal growth factor; Sigma, E4127), FGF2 [fibroblast growth factor 2 (basic); Invitrogen, PHG0026], B27 (Gibco, 17504-044), and heparin (Sigma, H6279). Results are presented as means ± standard deviation (SD) from 3 independent experiments. Primary mammospheres (2 or more cells) were counted. For limiting dilution mammosphere assays, 25 to 500 CD24$^+$ CD29^{hi} MECs per well were plated in duplicate.

The 3D colony-forming assays were performed as previously described.[23,25] 20,000 CD24$^+$ CD29^{hi} MECs per well were plated in reduced growth factor Matrigel (BD, 354230) and supplemented with mammary epithelial growth medium (MEGM) (Lonza, CC3051A), 5% FBS, EGF, and FGF2. Colonies were counted after 9 to 14 d. Results are presented as means ± SDs from 3 independent experiments.

The 2D colony-forming assays were performed as previously described.[23,25] 1,000 CD24$^+$ CD29^{lo} cells per well were plated on reduced growth factor Matrigel, supplemented with MEGM, 10% FBS, EGF, FGF2. Colonies were counted after 7 to 9 d. Results are presented as means ± SDs from 3 independent experiments.

Transplantation assays

MECs were isolated as previously described.[22] FACS was used to collect CD24$^+$ CD29^{hi} MECs, i.e., the MaSC-containing population, and transplantations were performed as previously described into cleared fat pads of 3- to 4-wk-old recipient wild-type C57BL/6 female mice,[22] in accordance with IACUC-approved protocols. Primary MEC donors were littermates. CD24$^+$ CD29^{hi} MECs were injected in a 200 μL volume (100 μL reduced growth factor Matrigel + 100 μL 1× phosphate-buffered saline (PBS; Gibco, 14190) at cell numbers specified. Mammary outgrowths were allowed to grow for 6 wk following transplantation and were then dissected, mounted on microscope slides, and processed for histological analysis. Three independent transplantation experiments were performed.

Mammary gland whole mounting

Native mammary glands from pubertal mice and mammary outgrowths generated by CD24$^+$ CD29^{hi} MEC transplantation were mounted onto microscope slides and fixed in 10% formalin overnight. Mammary glands from aged mice were mounted on microscope slides and fixed in Carnoy fixative for de-fatting. Mounts were then subjected to graded ethanol to water washes, and stained with carmine solution (Sigma, C1022 prepared as directed, with Aluminum Potassium Sulfate, Sigma, A7167) overnight with shaking. Stained slides were then subjected to graded water to ethanol washes, destained and stored in Histo-Clear II (National Diagnostics, HS-202). Imaging was done on Olympus SZ61 dissecting microscope (Rutgers Cancer Institute of New Jersey) using the ProRes Capture Pro2.5 software.

Stable cell lines and culture conditions

Cells were maintained in F12 (Gibco, 11765), 10% FBS, 1% penicillin/streptomycin, 5 ng/mL EGF, 1 μg/mL hydrocortisone (Sigma, H0888), 5 μg/mL insulin (Sigma, I9278). Cells were plated on glass coverslips, and allowed to attach overnight.

For immunofluorescence (IF), cells were fixed with 1:1 methanol: acetone at −20 °C for 10 min and rinsed with 1× PBS. Slides were incubated with 50 μL KRT6 primary antibody 1:200 in 3% bovine serum albumin (BSA; Benchmark, 100-106), 0.01% Tween 20 (BIO-RAD, 170-6531), 1× PBS at 37 °C for 90 min with shaking. After washing with 0.01% Tween 20, 1× PBS, slides were incubated with 50 μL FITC-conjugated anti-rabbit antibody (Jackson ImmunoResearch, 711-095-152) 1:100 in 3% BSA, 0.01% Tween 20, 1× PBS at 37 °C for 30 min with shaking. Cells were stained with DAPI (Invitrogen, P36931) and mounted with ProLong Gold Antifade Mounting Media (Life Technologies, P363930). Slides were imaged using the Olympus 1×51 scope and Metamorph Image program.

Primary MEC isolation and FACS for MEC subpopulations

Primary MECs were isolated as previously described.[22,23,25] MECs were stained as previously described[22,23] and sorted using FACSVantage SE with DiVa (BD) at Princeton University. LIN^- refers to cluster differentiation 31 $(CD31)^-$, cluster differentiation 45 $(CD45)^-$, and erythroid-specific LY76 (lymphocyte antigen 76)$^-$ negative cells, i.e. MECs. $CD24^+$ $CD29^{hi}$ MECs refer to a MaSC-containing population, $CD24^+$ $CD29^{lo}$ to a mammary progenitor cell-containing, and $CD24^-$ to differentiated MECs, as previously described.[22,23] FACS profiles were analyzed using FlowJo software (TreeStar, Inc.). Five independent experiments were performed.

Primary and stable cell lines

Immortalized mouse mammary epithelial cells were generated as previously described.[6] MaSC and MaPC colony- and mammosphere-forming assays were performed as previously described.[23,25] MaSC transplantations were performed as previously described.[22]

Histology of tissues and tumors

Mammary tissues were processed and imaged as previously described.[15] Following Carmine staining, mammary glands and outgrowths from $CD24^+$ $CD29^{hi}$ MEC transplantation were transferred to 70% ethanol overnight, and processed as above. Hematoxylin and eosin (H&E) staining and imaging were performed by the Histopathological and Imaging Core Facility at Rutgers Cancer Institute of New Jersey.

Antibodies

For flow cytommetry, CD31 (BD558737), CD45 (B553078), LY76/TER119 (BD553672), and CD24-PE (BD553262) antibodies were from BD Biosciences, CD61-APC (MCD6105) from Invitrogen, and CD29-FITC (MCA2298FB) from Serotech were used. For immunohistology, KRT6 (PRB-169P) from Covance, KRT17 (ab53707), TNF/TNFα (ab8871), F4/80 (ab6640), and 8-O-dG (ab48508) from Abcam, KRT14 (gift from Dr Segre), PGR (gift from Dr Clarke), CASP3 (9661) from Cell Signaling Technology, MKI67 (NCL-L-Ki67-MM1) from Leica, ESR1/ERα (sc-542) and RELA/p65 (sc-8008) from Santa Cruz Biotechnology, TNFRSF11A/TNR11 (AF692) and TNFSF11/TNF11 (AF462) from R&D Systems, SQSTM1 (BML-PW9860) from Enzo, LC3 (NB100-2331) and IL1B/IL-1β (NBP1-19775) from Novus Biologics, and KRT8 (TROMA-1) and BrdU (G3G4) from the Developmental Studies Hybridoma Bank were used.

Immunostaining

For immunohistochemistry (IHC), slides were deparrafinized with xylenes, rehydrated with ethanol to water washes, and boiled at 97 °C for 16 min in 1× Antigen Unmasking Solution (Vector, H-3300). For PGR staining, retrieval was done by autoclaving at 121 °C, 16 to 17psi, for 30 min in Vector 1× unmasking solution. For ESR1 staining, retrieval was done by microwaving slides in 1× Vector Unmasking Solution for 20 min. Slides were washed in water, followed by endogenous peroxidase blocking with 3% H_2O_2. Washes in 0.05% Tween 20 in 1× PBS or 0.05% Triton X-100 (Sigma, X100) (for PGR) were performed before blocking for 1 h at room temperature in 5% goat serum albumin for rabbit antibody, 5% BSA for goat antibody, or MOM Blocking Reagent (Vector, MKB-2213) for mouse or rat antibodies. For ESR1 staining, retrieval was done by microwaving slides in 1× Vector Unmasking Solution for 20 min. For rabbit and goat antibodies, primary antibodies were added in blocking reagent overnight at 4 °C. Biotin-conjugated anti-rabbit 1:1000 (Novus, NB 730-B) in 5% goat serum albumin (Jackson ImmunoResearch, 005-000-001)or anti-goat 1:500 (Jackson ImmunoResearch, 711-065-152) in 5% BSA were added to slides for 1 h at room temperature. For rat and mouse antibodies, primary antibodies were added in MOM diluent (prepared as per MKB-2202) for 30 min at room temperature as directed. For rat antibody, biotinylated anti-rat (Dako, E0468) 1:500 was added for 1 h at room temperature. For mouse antibody, biotinylated anti-mouse antibody (MKB-2225) 1:250 in MOM diluent was added at room temperature for 10 min (15 min for PGR). For all antibodies, sections were washed with 0.05% Tween 20 in 1× PBS, then incubated in Vector Elite ABC reagent (PK-7100) for 30 min at room temperature. For ESR1, an additional Streptavidin-HRP (Vector, SA-5704) incubation step was performed for 30 min as room temperature. All sections were incubated in DAB + chromogen substrate (Dako, K3468) for 10 min (15 min for PGR and ESR1), and counterstained with Harris Modified Hematoxylin 1:5 (Fischer Scientific, SH26-500D). Slides were mounted with Permount medium (Fisher Scientific, SP15-100). Imaging was done with an Olympus 1×51 microscope, Jenoptik Laser Optik camera system (Rutgers Cancer Institute of New Jersey), and ProgRes $C10^{Plus}$ software.

For immunofluorescence (IF), slides were deparrafinized with xylene, rehydrated with ethanol to 1× PBS washes, and boiled at 97 °C for 16 min in 1 M Urea (Bio-Rad, 161-0730) or 1× Vector Unmasking Solution (TNFSF11 only). For PGR staining, retrieval was done by autoclaving slides at 121 °C, 16 to 17 psi, for 30 min in 1× Vector Unmasking Solution. Slides were washed 4 times in water and once in 1× PBS, followed by blocking for 1 h at room temperature in 5% BSA (0.5% Tween-20, 1× PBS) or MOM Blocking Reagent (1× PBS for MKI67 and 0.05% Triton X-100, 1× PBS for PGR). Nonmouse primary antibodies were added in 5% BSA at room temperature for 2 h,

except for the TNFSF11 antibody, which was added in 1% BSA, 0.5% Tween 20 overnight at 4 °C. PGR antibody was used in MOM diluent in 0.05% Triton X-100, 1× PBS for 2 h at room temperature. Anti-rat, anti-chicken, and anti-rabbit fluorescent antibodies 1:100 (Jackson ImmunoResearch) were used in 5% BSA for 1 h at room temperature. For TNFSF11, biotinylated anti-goat 1:500 (Jackson ImmunoResearch, 711-065-152) was used for 1 h at room temperature, followed by streptavidin-Texas Red 1:100 (Invitrogen, SA1017) for 30 min. For PGR, biotinylated anti-mouse 1:250 in MOM diluent in 0.05% Triton X-100, 1× PBS was used at room temperature for 15 min, followed by streptavidin-Texas Red 1:100. For KRT6, CD29 and CD24 costaining, slides were first stained with KRT6 and CD29 antibodies, anti-rabbit Alexa-647 1:100 (Invitrogen, A20991) and anti-rat TRITC, then with the CD24-PE. After all antibody incubations, sections were washed with 1× PBS 3 times and mounted with ProLong Gold antifade with DAPI. Confocal imaging was done using the LSM510 Meta Confocal Laser Scanning Microscope at the Keck Collaborative Neuroscience Center at Rutgers University.

Data quantification and statistical analysis

For all in vitro studies statistics, 2-tailed Student *t* tests were performed using http://graphpad.com/quickcalcs/ttest1/. Immunostaining quantification was performed on at least 3 individual mammary gland specimens, including all TEBs and ducts per slide. For mammary side-branching quantification, results are presented as means with standard deviation (± SD) from 3 mammary gland specimens per genotype from C57BL/6 littermates. Same results were obtained in FVB/N background. For statistics on Kaplan Meier curves, Graph Prism software and Mantel-Cox analysis were utilized.

Mouse mammary tumor gene expression analysis

A minimum of 1 million cells were harvested and lysed directly from culture plates using 2 mL Trizol (Invitrogen, 15596-026). Cell lysates were incubated on ice for 5 min, then vortexed for 1 min. Tumors were dissected from mice and snap frozen in liquid nitrogen. Cell lysates and tumor specimens were given to the Functional Genomics Core Facility at Rutgers CINJ for RNA extraction and gene expression profiling on Affymetrix Mouse Genome 430 2.0 microarray. Using GeneSpring GX 11.5 (Agilent Technologies, Inc., Santa Clara, CA, USA), raw gene expression signals were summarized with MAS5. The data was further normalized using baseline transformation by the median of all samples and log scaling. Further, the normalized expression signals were averaged between biological replicates where applicable. Gene expression data was first filtered by flags (labeled as "present," "marginal," or "absent"). Probes were only kept if at least one sample was labeled as "present." Gene lists were generated by pair-wise comparison. Differentially expressed genes were designated by looking for a significant fold change (> 2.0) between the normalized expression values of 2 experiments. Genes were considered significantly stagnant if the fold change was low (< 1.25).

The generated gene list data were analyzed through the use of Ingenuity Pathways Analysis (Ingenuity® Systems, www.ingenuity.com). The Functional Analysis identified the biological functions and/or diseases that were most significant to the data set. Molecules from the data set that met the fold change cutoff of 2-fold and were associated with biological functions and/or diseases in Ingenuity's Knowledge Base were considered for the analysis. The right-tailed Fisher exact test was used to calculate a *P* value determining the probability that each biological function and/or disease assigned to that data set is due to chance alone.

Human breast cancer cohorts

The Sabatier[43] cohort included 266 breast tumor samples analyzed with Affymetrix U133 Plus 2.0 Arrays [PMID: 20490655]. The data was downloaded from Gene Expression Omnibus, series GSE21653. The Hatzis[42] cohort included 508 ERBB2-negative breast tumor samples analyzed with Affymetrix U133A Arrays [PMID: 21558518]. The data was downloaded from Gene Expression Omnibus, series GSE25066. Raw CEL files were processed using the justRMA function in R Bioconductor. The samples were classified into *BECN1* high or *BECN1* low depending on whether *BECN1* mRNA expression (probe 208945_s_at) was above or below the average across samples. WNT pathway gene signature was based on KEGG pathway: hsa04310 for WNT signaling pathway-Homo sapiens (http://www.genome.jp/dbget-bin/www_bget?_hsa04310). An activated WNT pathway gene signature was attributed to tumors with significant ($P < 0.05$) upregulation of WNT pathway gene signature expression relative to the rest of tumors within each breast cancer cohort; a Fischer exact test was used for this calculation.

Pathway gene signatures

Pathway gene expression signatures (according to KEGG pathway annotations) were analyzed using Gene Set Enrichment Analysis (GSEA) [PMID: 16199517]. For each sample and signature, GSEA reports a signature expression score between 0 and 1 and the statistical significance (*P* value) for signature overexpression. The statistical significance of upregulation of a given signature on a group of samples was determined using a Fischer exact test for enrichment of samples with significant ($P < 0.05$) signature expression in the group relative to samples outside the group.

Disclosure of Potential Conflicts of Interest

No potential conflicts of interest were disclosed.

Acknowledgments

We thank Z Yue and S Jin (Mount Sinai School of Medicine and Rutgers University), Dr Komatsu (Tokyo Metropolitan Institute of Medical Science), Dr Mizushima (University of Tokyo), and Y Li (Baylor College of Medicine) for providing *Becn1*$^{+/-}$, *Atg7*$^{F/F}$, GFP-LC3B, and MMTV-*Wnt1* mice, respectively. We thank Dr Segre (National Institute of Health) for the KRT14 antibody and Dr Clarke (Westmead Millennium Institute) for the PGR antibody. We also thank N Goldsmith-Kane for assistance with confocal microscopy, the Histopathological, Imaging, and Functional Genomics Core Facilities at Rutgers Cancer Institute of New Jersey; also, the Flow Cytometry Facility at Princeton University. We are indebted to Ed and Sue

Goldstein for their unconditional support and encouragement. This work is dedicated to the memory of Stacy Goldstein.

Funding

We are grateful for financial support from a New Jersey Commission on Cancer Research Predoctoral Fellowship (MC), NIH grant R00-CA133181 (VK) and a Damon Runyon Clinical Investigator Award (VK).

Supplemental Material

Supplemental data for this article can be accessed on the publisher's website.

References

1. Mizushima N, Levine B, Cuervo AM, Klionsky DJ. Autophagy fights disease through cellular self-digestion. Nature 2008; 451:1069–75; http://dx.doi.org/10.1038/nature06639; PMID:18305538
2. Aita VM, Liang XH, Murty VV, Pincus DL, Yu W, Cayanis E, Kalachikov S, Gilliam TC, Levine B. Cloning and genomic organization of beclin 1, a candidate tumor suppressor gene on chromosome 17q21. Genomics 1999; 59:59–65; PMID:10395800; http://dx.doi.org/10.1006/geno.1999.5851
3. Liang XH, Jackson S, Seaman M, Brown K, Kempkes B, Hibshoosh H, Levine B. Induction of autophagy and inhibition of tumorigenesis by beclin 1. Nature 1999; 402:672–6; http://dx.doi.org/10.1038/45257; PMID:10604474
4. Qu X, Yu J, Bhagat G, Furuya N, Hibshoosh H, Troxel A, Rosen J, Eskelinen EL, Mizushima N, Ohsumi Y, et al. Promotion of tumorigenesis by heterozygous disruption of the beclin 1 autophagy gene. J Clin Invest 2003; 112:1809–20; http://dx.doi.org/10.1172/JCI20039; PMID:14638851
5. Yue Z, Jin S, Yang C, Levine AJ, Heintz N. Beclin 1, an autophagy gene essential for early embryonic development, is a haploinsufficient tumor suppressor. Proc Natl Acad Sci U S A 2003; 100:15077–82; http://dx.doi.org/10.1073/pnas.2436255100; PMID:14657337
6. Karantza-Wadsworth V, Patel S, Kravchuk O, Chen G, Mathew R, Jin S, White E. Autophagy mitigates metabolic stress and genome damage in mammary tumorigenesis. Genes Dev 2007; 21:1621–35; PMID:17606641; http://dx.doi.org/10.1101/gad.1565707
7. Rosenfeldt MT, O'Prey J, Morton JP, Nixon C, MacKay G, Mrowinska A, Au A, Rai TS, Zheng L, Ridgway R, et al. p53 status determines the role of autophagy in pancreatic tumour development. Nature 2013; 504:296–300; http://dx.doi.org/10.1038/nature12865; PMID:24305049
8. Lozy F, Cai-McRae X, Teplova I, Price S, Reddy A, Bhanot G, Ganesan S, Vazquez A, Karantza V. ERBB2 overexpression suppresses stress-induced autophagy and renders ERBB2-induced mammary tumorigenesis independent of monoallelic Becn1 loss. Autophagy 2014; 10:662–76; PMID:24492513; http://dx.doi.org/10.4161/auto.27867
9. Wei Y, Zou Z, Becker N, Anderson M, Sumpter R, Xiao G, Kinch L, Koduru P, Christudass CS, Veltri RW, et al. EGFR-mediated Beclin 1 phosphorylation in autophagy suppression, tumor progression, and tumor chemoresistance. Cell 2013; 154:1269–84; http://dx.doi.org/10.1016/j.cell.2013.08.015; PMID:24034250
10. Gong C, Bauvy C, Tonelli G, Yue W, Deloménie C, Nicolas V, Zhu Y, Domergue V, Marin-Esteban V, Tharinger H, et al. Beclin 1 and autophagy are required for the tumorigenicity of breast cancer stem-like/progenitor cells. Oncogene 2013; 32:2261-72, 1-11; PMID:22733132; http://dx.doi.org/10.1038/onc.2012.252
11. Guo JY, Karsli-Uzunbas G, Mathew R, Aisner SC, Kamphorst JJ, Strohecker AM, Chen G, Price S, Lu W, Teng X, et al. Autophagy suppresses progression of K-ras-induced lung tumors to oncocytomas and maintains lipid homeostasis. Genes Dev 2013; 27:1447–61; http://dx.doi.org/10.1101/gad.219642.113; PMID:23824538
12. Strohecker AM, Guo JY, Karsli-Uzunbas G, Price SM, Chen GJ, Mathew R, McMahon M, White E. Autophagy sustains mitochondrial glutamine metabolism and growth of BrafV600E-driven lung tumors. Cancer Discov 2013; 3:1272–85; PMID:23965987; http://dx.doi.org/10.1158/2159-8290.CD-13-0397
13. Huo Y, Cai H, Teplova I, Bowman-Colin C, Chen G, Price S, Barnard N, Ganesan S, Karantza V, White E, et al. Autophagy opposes p53-mediated tumor barrier to facilitate tumorigenesis in a model of PALB2-associated hereditary breast cancer. Cancer Discov 2013; 3:894–907; http://dx.doi.org/10.1158/2159-8290.CD-13-0011; PMID:23650262
14. Wei H, Wei S, Gan B, Peng X, Zou W, Guan JL. Suppression of autophagy by FIP200 deletion inhibits mammary tumorigenesis. Genes Dev 2011; 25:1510–27; http://dx.doi.org/10.1101/gad.2051011; PMID:21764854
15. Teplova I, Lozy F, Price S, Singh S, Barnard N, Cardiff RD, Birge RB, Karantza V. ATG proteins mediate efferocytosis and suppress inflammation in mammary involution. Autophagy 2013; 9:459–75; http://dx.doi.org/10.4161/auto.23164; PMID:23380905
16. Laddha SV, Ganesan S, Chan CS, White E. Mutational landscape of the essential autophagy gene BECN1 in human cancers. Mol Cancer Res 2014; 12:485–90; PMID:24478461; http://dx.doi.org/10.1158/1541-7786.MCR-13-0614
17. Kongara S, Kravchuk O, Teplova I, Lozy F, Schulte J, Moore D, Barnard N, Neumann CA, White E, Karantza V. Autophagy regulates keratin 8 homeostasis in mammary epithelial cells and in breast tumors. Mol Cancer Res 2010; 8:873–84; http://dx.doi.org/10.1158/1541-7786.MCR-09-0494; PMID:20530580
18. Li Y, Welm B, Podsypanina K, Huang S, Chamorro M, Zhang X, Rowlands T, Egeblad M, Cowin P, Werb Z, et al. Evidence that transgenes encoding components of the Wnt signaling pathway preferentially induce mammary cancers from progenitor cells. Proc Natl Acad Sci U S A 2003; 100:15853–8; http://dx.doi.org/10.1073/pnas.2136825100; PMID:14668450
19. Bu W, Chen J, Morrison GD, Huang S, Creighton CJ, Huang J, Chamness GC, Hilsenbeck SG, Roop DR, Leavitt AD, et al. Keratin 6a marks mammary bipotential progenitor cells that can give rise to a unique tumor model resembling human normal-like breast cancer. Oncogene 2011; 30:4399–409; http://dx.doi.org/10.1038/onc.2011.147; PMID:21532625
20. Liu BY, McDermott SP, Khwaja SS, Alexander CM. The transforming activity of Wnt effectors correlates with their ability to induce the accumulation of mammary progenitor cells. Proc Natl Acad Sci U S A 2004; 101:4158–63; http://dx.doi.org/10.1073/pnas.0400699101; PMID:15020770
21. Grimm SL, Bu W, Longley MA, Roop DR, Li Y, Rosen JM. Keratin 6 is not essential for mammary gland development. Breast Cancer Res 2006; 8:R29; PMID:16790075; http://dx.doi.org/10.1186/bcr1504
22. Shackleton M, Vaillant F, Simpson KJ, Stingl J, Smyth GK, Asselin-Labat ML, Wu L, Lindeman GJ, Visvader JE. Generation of a functional mammary gland from a single stem cell. Nature 2006; 439:84–8; http://dx.doi.org/10.1038/nature04372; PMID:16397499
23. Stingl J, Eirew P, Ricketson I, Shackleton M, Vaillant F, Choi D, Li HI, Eaves CJ. Purification and unique properties of mammary epithelial stem cells. Nature 2006; 439:993–7; http://dx.doi.org/10.1038/nature04496; PMID:16395311
24. Vaillant F, Asselin-Labat ML, Shackleton M, Forrest NC, Lindeman GJ, Visvader JE. The mammary progenitor marker CD61/beta3 integrin identifies cancer stem cells in mouse models of mammary tumorigenesis. Cancer Res 2008; 68:7711–7; http://dx.doi.org/10.1158/0008-5472.CAN-08-1949; PMID:18829523
25. Dontu G, Abdallah WM, Foley JM, Jackson KW, Clarke MF, Kawamura MJ, Wicha MS. In vitro propagation and transcriptional profiling of human mammary stem/progenitor cells. Genes Dev 2003; 17:1253–70; http://dx.doi.org/10.1101/gad.1061803; PMID:12756227
26. Komatsu M, Waguri S, Ueno T, Iwata J, Murata S, Tanida I, Ezaki J, Mizushima N, Ohsumi Y, Uchiyama Y, et al. Impairment of starvation-induced and constitutive autophagy in Atg7-deficient mice. J Cell Biol 2005; 169:425–34; http://dx.doi.org/10.1083/jcb.200412022; PMID:15866887
27. Jonkers J, Meuwissen R, van der Gulden H, Peterse H, van der Valk M, Berns A. Synergistic tumor suppressor activity of BRCA2 and p53 in a conditional mouse model for breast cancer. Nat Genet 2001; 29:418–25; http://dx.doi.org/10.1038/ng747; PMID:11694875
28. Joshi PA, Jackson HW, Beristain AG, Di Grappa MA, Mote PA, Clarke CL, Stingl J, Waterhouse PD, Khokha R. Progesterone induces adult mammary stem cell expansion. Nature 2010; 465:803–7; http://dx.doi.org/10.1038/nature09091; PMID:20445538
29. Gonzalez-Suarez E, Branstetter D, Armstrong A, Dinh H, Blumberg H, Dougall WC. RANK overexpression in transgenic mice with mouse mammary tumor virus promoter-controlled RANK increases proliferation and impairs alveolar differentiation in the mammary epithelia and disrupts lumen formation in cultured epithelial acini. Mol Cell Biol 2007; 27:1442–54; http://dx.doi.org/10.1128/MCB.01298-06; PMID:17145767
30. Fernandez-Valdivia R, Mukherjee A, Ying Y, Li J, Paquet M, DeMayo FJ, Lydon JP. The RANKL signaling axis is sufficient to elicit ductal side-branching and alveologenesis in the mammary gland of the virgin mouse. Dev Biol 2009; 328:127–39; http://dx.doi.org/10.1016/j.ydbio.2009.01.019; PMID:19298785
31. Darnay BG, Ni J, Moore PA, Aggarwal BB. Activation of NF-kappaB by RANK requires tumor necrosis factor receptor-associated factor (TRAF) 6 and NF-kappaB-inducing kinase. Identification of a novel TRAF6 interaction motif. J Biol Chem 1999; 274:7724–31; PMID:10075662; http://dx.doi.org/10.1074/jbc.274.12.7724
32. Asselin-Labat ML, Vaillant F, Sheridan JM, Pal B, Wu D, Simpson ER, Yasuda H, Smyth GK, Martin TJ, Lindeman GJ, et al. Control of mammary stem cell function by steroid hormone signalling. Nature 2010; 465:798–802; http://dx.doi.org/10.1038/nature09027; PMID:20383121
33. Dougall WC. RANKL signaling in bone physiology and cancer. Curr Opin Support Palliat Care 2007; 1:317–22; http://dx.doi.org/10.1097/SPC.0b013e3282f335be; PMID:18685382
34. Gonzalez-Suarez E, Jacob AP, Jones J, Miller R, Roudier-Meyer MP, Erwert R, Pinkas J, Branstetter D, Dougall WC. RANK ligand mediates progestin-induced mammary epithelial proliferation and carcinogenesis. Nature 2010; 468:103–7; http://dx.doi.org/10.1038/nature09495; PMID:20881963

35. Lydon JP, DeMayo FJ, Conneely OM, O'Malley BW. Reproductive phenotpes of the progesterone receptor null mutant mouse. J Steroid Biochem Mol Biol 1996; 56:67–77; PMID:8603049; http://dx.doi.org/10.1016/0960-0760(95)00254-5
36. Takayanagi H, Sato K, Takaoka A, Taniguchi T. Interplay between interferon and other cytokine systems in bone metabolism. Immunol Rev 2005; 208:181–93; http://dx.doi.org/10.1111/j.0105-2896.2005.00337.x; PMID:16313349
37. Kongara S, Karantza V. The interplay between autophagy and ROS in tumorigenesis. Front Oncol 2012; 2:171; PMID:23181220
38. Davie SA, Maglione JE, Manner CK, Young D, Cardiff RD, MacLeod CL, Ellies LG. Effects of FVB/NJ and C57Bl/6J strain backgrounds on mammary tumor phenotype in inducible nitric oxide synthase deficient mice. Transgenic Res 2007; 16:193–201; http://dx.doi.org/10.1007/s11248-006-9056-9; PMID:17206489
39. Visvader JE. Cells of origin in cancer. Nature 2011; 469:314–22; http://dx.doi.org/10.1038/nature09781; PMID:21248838
40. Li Y, Hively WP, Varmus HE. Use of MMTV-Wnt-1 transgenic mice for studying the genetic basis of breast cancer. Oncogene 2000; 19:1002–9; http://dx.doi.org/10.1038/sj.onc.1203273; PMID:10713683
41. Liu J, Xia H, Kim M, Xu L, Li Y, Zhang L, Cai Y, Norberg HV, Zhang T, Furuya T, et al. Beclin1 controls the levels of p53 by regulating the deubiquitination activity of USP10 and USP13. Cell 2011; 147:223–34; http://dx.doi.org/10.1016/j.cell.2011.08.037; PMID:21962518
42. Hatzis C, Pusztai L, Valero V, Booser DJ, Esserman L, Lluch A, Vidaurre T, Holmes F, Souchon E, Wang H, et al. A genomic predictor of response and survival following taxane-anthracycline chemotherapy for invasive breast cancer. JAMA 2011; 305:1873–81; http://dx.doi.org/10.1001/jama.2011.593; PMID:21558518
43. Sabatier R, Finetti P, Cervera N, Lambaudie E, Esterni B, Mamessier E, Tallet A, Chabannon C, Extra JM, Jacquemier J, et al. A gene expression signature identifies two prognostic subgroups of basal breast cancer. Breast Cancer Res Treat 2011; 126:407–20; http://dx.doi.org/10.1007/s10549-010-0897-9; PMID:20490655
44. Shravage BV, Hill JH, Powers CM, Wu L, Baehrecke EH. Atg6 is required for multiple vesicle trafficking pathways and hematopoiesis in Drosophila. Development 2013; 140:1321–9; http://dx.doi.org/10.1242/dev.089490; PMID:23406899
45. Wang C, Liang CC, Bian ZC, Zhu Y, Guan JL. FIP200 is required for maintenance and differentiation of postnatal neural stem cells. Nat Neurosci 2013; 16:532–42; http://dx.doi.org/10.1038/nn.3365; PMID:23542691
46. Schramek D, Leibbrandt A, Sigl V, Kenner L, Pospisilik JA, Lee HJ, Hanada R, Joshi PA, Aliprantis A, Glimcher L, et al. Osteoclast differentiation factor RANKL controls development of progestin-driven mammary cancer. Nature 2010; 468:98–102; http://dx.doi.org/10.1038/nature09387; PMID:20881962
47. Palafox M, Ferrer I, Pellegrini P, Vila S, Hernandez-Ortega S, Urruticoechea A, Climent F, Soler MT, Muñoz P, Viñals F, et al. RANK induces epithelial-mesenchymal transition and stemness in human mammary epithelial cells and promotes tumorigenesis and metastasis. Cancer Res 2012; 72:2879–88; http://dx.doi.org/10.1158/0008-5472.CAN-12-0044; PMID:22496457
48. Kühn MC, Willenberg HS, Schott M, Papewalis C, Stumpf U, Flohé S, Scherbaum WA, Schinner S. Adipocyte-secreted factors increase osteoblast proliferation and the OPG/RANKL ratio to influence osteoclast formation. Mol Cell Endocrinol 2012; 349:180–8; http://dx.doi.org/10.1016/j.mce.2011.10.018; PMID:22040599
49. Bendre M, Gaddy D, Nicholas RW, Suva LJ. Breast cancer metastasis to bone: it is not all about PTHrP. Clin Orthop Relat Res 2003; (Suppl):S39–45; http://dx.doi.org/10.1097/01.blo.0000093844.72468.f4; PMID:14600591
50. Takamura A, Komatsu M, Hara T, Sakamoto A, Kishi C, Waguri S, Eishi Y, Hino O, Tanaka K, Mizushima N. Autophagy-deficient mice develop multiple liver tumors. Genes Dev 2011; 25:795–800; http://dx.doi.org/10.1101/gad.2016211; PMID:21498569
51. Mariño G, Salvador-Montoliu N, Fueyo A, Knecht E, Mizushima N, López-Otín C. Tissue-specific autophagy alterations and increased tumorigenesis in mice deficient in Atg4C/autophagin-3. J Biol Chem 2007; 282:18573–83; PMID:17442669; http://dx.doi.org/10.1074/jbc.M701194200
52. Cook KL, Shajahan AN, Clarke R. Autophagy and endocrine resistance in breast cancer. Expert Rev Anticancer Ther 2011; 11:1283–94; http://dx.doi.org/10.1586/era.11.111; PMID:21916582
53. Alexander CM, Goel S, Fakhraldeen SA, Kim S. Wnt signaling in mammary glands: plastic cell fates and combinatorial signaling. Cold Spring Harb Perspect Biol 2012; 4: http://dx.doi.org/10.1101/cshperspect.a008037; PMID:22661590
54. Bertrand FE, Angus CW, Partis WJ, Sigounas G. Developmental pathways in colon cancer: crosstalk between WNT, BMP, Hedgehog and Notch. Cell Cycle 2012; 11:4344–51; http://dx.doi.org/10.4161/cc.22134; PMID:23032367
55. Howe LR, Brown AM. Wnt signaling and breast cancer. Cancer Biol Ther 2004; 3:36–41; PMID:14739782; http://dx.doi.org/10.4161/cbt.3.1.561
56. Geyer FC, Lacroix-Triki M, Savage K, Arnedos M, Lambros MB, MacKay A, Natrajan R, Reis-Filho JS. β-Catenin pathway activation in breast cancer is associated with triple-negative phenotype but not with CTNNB1 mutation. Mod Pathol 2011; 24:209–31; http://dx.doi.org/10.1038/modpathol.2010.205; PMID:21076461
57. Alanazi MS, Parine NR, Shaik JP, Alabdulkarim HA, Ajaj SA, Khan Z. Association of single nucleotide polymorphisms in Wnt signaling pathway genes with breast cancer in Saudi patients. PLoS One 2013; 8:e59555; http://dx.doi.org/10.1371/journal.pone.0059555; PMID:23516639
58. Benhaj K, Akcali KC, Ozturk M. Redundant expression of canonical Wnt ligands in human breast cancer cell lines. Oncol Rep 2006; 15:701–7; PMID:16465433
59. Goessl C, Katz L, Dougall WC, Kostenuik PJ, Zoog HB, Braun A, Dansey R, Wagman RB. The development of denosumab for the treatment of diseases of bone loss and cancer-induced bone destruction. Ann N Y Acad Sci 2012; 1263:29–40; http://dx.doi.org/10.1111/j.1749-6632.2012.06674.x; PMID:22831177
60. Liu X, Holstege H, van der Gulden H, Treur-Mulder M, Zevenhoven J, Velds A, Kerkhoven RM, van Vliet MH, Wessels LF, Peterse JL, et al. Somatic loss of BRCA1 and p53 in mice induces mammary tumors with features of human BRCA1-mutated basal-like breast cancer. Proc Natl Acad Sci U S A 2007; 104:12111–6; http://dx.doi.org/10.1073/pnas.0702969104; PMID:17626182